Geomorphology 464 (2024) 109374

Contents lists available at ScienceDirect

Geomorphology

journal homepage: www.journals.elsevier.com/geomorphology

Tectonic geomorphology and deep-seated gravitational slope deformations (DSGSDs) in the Acıgöl Graben, Türkiye

Esra Tunçel [a,*], Francisco Gutiérrez [b], Ergin Gökkaya [c], Gürol Seyitoğlu [d], İhsan Çiçek [e]

[a] Department of Geography, Bilecik Şeyh Edebali University, Bilecik, Türkiye
[b] Department of Earth Sciences, University of Zaragoza, Pedro Cerbuna 12, 50009 Zaragoza, Spain
[c] Department of Geography, Niğde Ömer Halis Demir University, Niğde, Türkiye
[d] Department of Geological Engineering, Tectonics Research Group, Ankara University, Ankara, Türkiye
[e] Department of Geography, Ankara University, Ankara, Türkiye

ARTICLE INFO

Keywords:
Active normal faulting
Seismic hazard
Sackung
Landslide
Solution sinkholes

ABSTRACT

The Söğüt Mountains is a fault-bounded carbonate range situated between the active Acıgöl and Akgöl grabens in southwestern Türkiye. The southwestern sector of the Acıgöl Graben floor displays an array of faults that have produced peculiar intra-basin half-grabens with local lakes and drainages. The conspicuous geomorphic expression of the intra-basin faults and depressions in this sector of the basin is attributed to low sedimentation rate (i.e., starved basin) related to very limited runoff and sediment supply from the southwestern carbonate margin of the basin, dominated by subsurface drainage in a carbonate bedrock strongly affected by gravitational deformation and karstification. Detailed mapping reveals the presence of large landslides and extensive DSGSDs in the mountain fronts flanking the Söğüt Mountains, showing ridge-top depression, uphill-facing scarps, high-relief downhill-facing scarps, and toe bulges. Cartographic relationships provide insights into the development and evolution of the deformations in the slopes that experience continuous tectonic rejuvenation and debuttressing. DSGSDs and large landslides take advantage of secondary synthetic tectonic faults, in which gravitational and tectonic displacement are superposed. The transformation of DSGSDs into large to giant short runout landslides (up to ca. 3.5 Gm^3) occurs mainly on laterally unconfined slopes associated with bends and stepovers in the basin-bounding faults. Seismicity is likely the main triggering factor controlling the kinematics of the gravitational deformations and landslides. Cartographic evidence indicate downslope propagation of the gravitational deformation (uphill-facing-scarps and associated troughs) in the tectonically growing slopes. Additionally, preferential development of solution sinkholes is observed in gravitationally distorted slopes with impeded surface drainage.

1. Introduction

The antagonistic interplay between active tectonic processes, which tend to create relief, and erosional and aggradational processes that tend to degrade it, constitutes the core of tectonic geomorphology (Burbank and Anderson, 2008). The geomorphic impact of these competing endogenous and exogenous processes is particularly prominent in extensional terrains, where uplifted areas are dominated by erosion (e.g., fluvial incision, landsliding), while sediment aggradation occurs in subsiding basins. The evolution of normal faults through fault displacement, propagation and linkage can cause dramatic changes in the drainage network (e.g, Trudgill, 2002) and exerts a long-term control on the architecture of basin fills (Cowie et al., 2000). Thus, knowledge derived from the study of active extensional basins, including both the erosional margins (i.e., sediment sources) and aggradational floors, is of prime importance for understanding landscape evolution and inferring the history of ancient sedimentary basins (Leeder and Jackson, 1993; Gawthorpe and Leeder, 2000).

Deep-seated gravitational slope deformations (DSGSDs) refer to a range of morpho-structural features such as ridge-top depressions, uphill-facing scarps and associated troughs, downhill-facing scarps, or outward bulges related to gravity-driven deformation of rock slopes (Agliardi et al., 2001). This phenomenon typically occurs on high-relief slopes and is characterized by very slow average displacement rates (mm/year) (Agliardi et al., 2001; 2012; Agliardi and Crippa, 2022). It has been documented on slopes underlain by a wide variety of

* Corresponding author.
E-mail address: esra.tuncel@bilecik.edu.tr (E. Tunçel).

https://doi.org/10.1016/j.geomorph.2024.109374
Received 28 May 2024; Received in revised form 4 August 2024; Accepted 6 August 2024
Available online 8 August 2024

lithologies such as metamorphic, igneous, or layered sedimentary rocks (Agliardi and Crosta, 2012). Nevertheless, the existing literature includes a reduced number of cases in carbonate rocks (e.g., Pánek et al., 2009; Esposito et al., 2007; Gori et al., 2014), like the ones addressed in this work, despite the high spatial frequency of this lithology in mountainous terrains (Crosta et al., 2013; Goldscheider et al., 2020). For instance, Agliardi et al. (2012) produced a comprehensive cartographic inventory of 904 DSGSDs across the European Alps, with only a few occurrences in carbonate rocks, despite exposures of carbonate rocks represent 52 % of the analyzed region (Kellerer-Pirklbauer et al., 2022).

Numerous examples illustrate the strong control played by discontinuity planes (e.g., bedding, jointing, cleavage, faults) and their attitude on the distribution and failure mechanisms of DSGSDs (e.g., McCalpin and Irvine, 1995; Agliardi et al., 2001; Ambrosi and Crosta, 2006; Agliardi et al., 2009; Pánek et al., 2011). DSGSDs typically display discrete extensional morpho-structures in the upper part of the slopes (i.e., troughs bounded by normal fault scarps), which tend to be counterbalanced by compressional deformation in the lower part of the slope by continuous bulging, buckle folding, and fracturing (Chigira, 1992; Crosta et al., 2013; Jaboyedoff et al., 2013). A prominent feature often found on the crestal zone are ridge-top depressions that split the divides into two ridges, which have been designated by various terms such as double ridge (e.g., Agliardi et al., 2009) or *doppelgrat* (e.g., Zischinsky, 1969). In some cases, these gravitational ridge-top grabens host ephemeral ponds (Varnes et al., 1989). Uphill-facing scarps, also known as counter scarps, antislope scarps, and antithetic scarps (e.g., Radbruch-Hall et al., 1976; Agliardi et al., 2001; Březný et al., 2018) are probably the most common landform observable in the upper part of DSDSDs. These scarps are typically oriented parallel to the contour lines and may show a slight outward convexity (e.g., Varnes et al., 1989). Troughs with internal drainage may form on the upslope side of these scarps and small collapse sinkholes have been observed within these linear depressions, even in the absence of soluble rock (i.e., ravelling of cover deposits into dilated discontinuities; Bovis, 1982; McCalpin and Irvine, 1995; Gutiérrez et al., 2008). In some cases, slopes disrupted by multiple contour-parallel ruptures exhibit a serrated topography featuring multiple ridges and linear depressions (McCalpin and Hart, 2002; Crosta et al., 2013; Fioraso, 2017). Downhill-facing scarps can also be found, which may display an outward-facing concave trace, resembling the headscar of an “incomplete” landslide (McCalpin and Irvine, 1995; Agliardi et al., 2001; McCalpin and Hart, 2002; Gutiérrez-Santolalla et al., 2005).

DSGSDs have been documented in diverse settings, such as glaciated mountain regions (Agliardi et al., 2001), seismically active areas (Beck, 1968; Solonenko, 1977; Radbruch-Hall, 1978) and slopes underlain by soluble rocks (Pánek et al., 2009; Gutiérrez et al., 2012a). However, studies addressing this type of slope movements in mountain fronts associated with active normal faults (e.g., McCalpin and Jones, 2021) or reverse faults (e.g., McCalpin et al., 2020) are scarce. Specific factors that can favor or initiate DSGSDs are linked to the different geomorphic settings. For instance, tensile stress on the upper sectors of steep ridges (Radbruch-Hall, 1978), loss of lateral confining pressure related to the retreat of valley glaciers (Agliardi et al., 2001), or dynamic loading related to the seismic shaking (Beck, 1968; Solonenko, 1977; Radbruch-Hall, 1978) have all been proposed as potential preparatory or triggering factors. The link between large earthquakes and the occurrence or reactivation of DSGSDs is well supported by numerous historical events. These include historical reactivation of a gravitational fault scarp in a ridge-top depression in the Stillwater Range, Nevada, during the 1915 Pleasant Valley earthquake (Mw 7.3) and the 1954 Dixie Valley-Fairview Peak earthquakes (Mw 6.8 and 7.2) (McCalpin and Jones, 2021), the 1989, M_w 6.9 Loma Prieta earthquake in California (Cotton et al., 1989; Hart et al., 1989; Ponti and Wells, 1991), the 1997 seismic sequence (M_w 5.7 to 6) in central Italy (Moro et al., 2007), and the 2002, M_w 7.9 Denali earthquake in Alaska (Jibson et al., 2004). Furthermore, trenching studies conducted across troughs in tectonically active regions have provided evidence of episodic displacement, supporting earthquake-related events (McCalpin and Hart, 2002; Gutiérrez-Santolalla et al., 2005; Gutiérrez et al., 2008; Moro et al., 2012). Displacement events can be triggered by nearby seismic activity, and the magnitude, epicentral distance, and direction of earthquakes have effect on the displacement (McCalpin and Jones, 2021). The contemporaneity between displacement events in DSGSDs and large earthquakes needs to be substantiated with numerical ages that commonly require trenching investigations (Komura et al., 2020).

Linear scarps documented in seismically active regions have been interpreted differently in successive studies, some attributing them to gravitational deformation and others to seismogenic tectonic faults deeply rooted in the crust. For instance, long, linear antislope scarps in the crest of Mount Currie (British Columbia) have been interpreted as either young fault scarps resulting from tectonic activity, or gravitational failures due to toppling and nonseismogenic gravity-driven processes (McCalpin, 1999 and references therein). Similar debates exist in relation to other scarps, such as the 3 km long exposed fault scarps in the Apennines, where interpretations range from recent activity on a slope-bounding fault (Roberts and Michetti, 2004) to a gravitational failure (Galadini, 2006). Likewise, a 1.5 km long linear scarp on Middagstinden Mountain in western Norway has been interpreted as evidence of a Holocene fault (Anda et al., 2002) while, other studies advocate for a gravitational origin (Krieger et al., 2013; Schleier et al., 2016). Distinguishing between gravitational deformations and tectonic structures is critical for seismic hazard assessment (e.g., Carbonel et al., 2013). The situation can be complicated when the slip surface of a gravitational deformation coincides with an active fault plane with dip-slip displacement component (e.g., Forcella and Orombelli, 1984; Gori et al., 2014). In such cases, displacement associated with gravitational slip is added to tectonic displacement on the upper part of the tectonic fault, potentially leading to neotectonic and paleoseismological misinterpretations (Gori et al., 2014; Galadini, 2006) such as slip rate, earthquake recurrence, or displacement-per-event. In addition, inactive tectonic faults can be reactivated by gravitational slip (Agliardi et al., 2001; Agliardi et al., 2009; Lebourg et al., 2011), which may lead to seismic hazard overestimations in case they are misinterpreted as seismogenic. On the other hand, gravitational deformation has the potential to obliterate features related to active faults (Agliardi et al., 2001; Agliardi et al., 2009), conceivable undervaluing seismic hazard.

A useful criterion for differentiating gravitational from tectonic fault scarps is the scarp height to scarp length ratio (McCalpin, 1999; Gutiérrez et al., 2012a, 2012b). Gravity-driven scarps tend to be much shorter for a given height compared to those formed by tectonic activity. Additionally, gravitational features often exhibit distinct characteristics; they are typically shorter, discontinuous, arcuate, may form closely-spaced parallel swarms and tend to align with the topographic trend (McCalpin, 1999). Conversely, tectonic fault scarps tend to have a more consistent trend and are longer, more linear, continuous, and typically occur as singular features (McCalpin, 1999). Local topography can also provide valuables clues; gravitational scarps typically occur in the upper slope sections, whereas tectonic dip-slip faults tend to occur at the foot of the slopes in fault-bounded blocks (McCalpin, 1999; Galadini, 2006). Examining the shear zones can provide further clues. DSGSDs, due to the downward movement of rock blocks, are expected to have asymmetric shear zones (Chigira, 1992), while tectonic faults tend to show symmetrical shear zones (McCalpin, 1999).

Another crucial aspect of DSGSDs concerns their potential to evolve into catastrophic landslides. Several studies suggest that landslides can be the final stage in a continuous evolution of DSGSDs (McCalpin and Hart, 2002; Gutiérrez et al., 2008; Agliardi et al., 2012; Kaneda and Kono, 2017). This concept is supported by documented cases in which DSGSDs preceded catastrophic landslides (Wang et al., 2003; Chigira et al., 2003; Sakals et al., 2012; Nishii et al., 2013). For instance, the head scarp of the Daguangbao landslide, triggered by the 2008 Wenchuan earthquake in China, coincided with a 2 km long ridge-top

depression (Chigira et al., 2010). Pánek and Klimeš (2016) examine recent catastrophic failures preceded by prolonged deep-seated deformation. They identified two main conditions associated with DSGSDs that predispose slopes to landslides: (1) reduction in rock-mass strength related to processes such as fragmentation and tilting of rocks into unstable positions; and (2) changes in slope topography, particularly bulging or buckling folding that leads to toe over-steepening and the creation of new water runoff paths (Pánek and Klimeš, 2016 and references therein).

Progressive development of DSGSDs was documented in the La

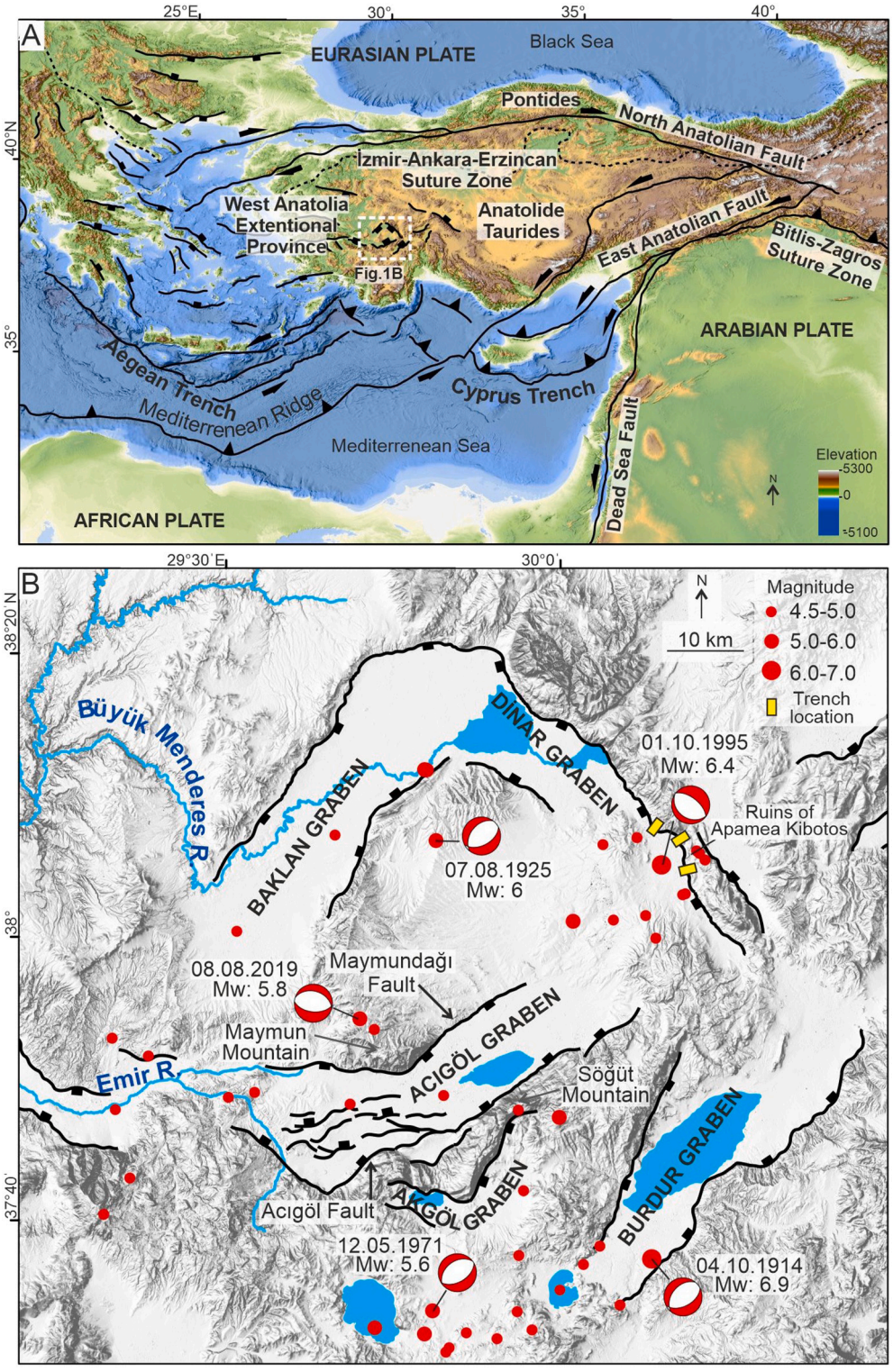

Fig. 1. A. Geotectonic context of the Eastern Mediterranean region associated with the Arabian, African, and Eurasian plates. Faults adapted from Seyitoğlu et al. (2022a, 2022b). Digital elevation model obtained from the GEBCO grid. The location of trenches reported by Altunel et al. (1999) and Kürçer et al. (2021) is shown. B. Hillshade showing the distribution of grabens in the vicinity of the Acıgöl Graben. Instrumentally recorded earthquakes with magnitude $M_s \geq 4.5$ are depicted as red circles. Specific earthquakes referred to in the text are labelled with their respective dates. Focal mechanism solutions indicative of normal faulting obtained from U.S. Geological Survey (2023), Taymaz and Price (1992) and Kılıç et al. (2017), digital elevation model obtained from Turkish General Directorate of Mapping.

Clapière slope movement (French Alps), where deformation started at the upper part of the slope with low displacement rates and propagated downwards with increasing displacement rates, and eventually intense shear stress concentration in the toe resulted in failure along a pre-existing tectonic structure (El Bedoui et al., 2009; Guglielmi and Cappa, 2010; Lebourg et al., 2011). Some examples from formerly glaciated regions have shown an opposite deformation pattern with upslope migration of extensional strain related to glacial oversteepening and debutressing (Bovis, 1982; Pánek et al., 2017; McCalpin and Corominas, 2019). The tectonic setting of a region significantly influences on the occurrence of DSGSDs and nested landslides through gravitational reactivation and progressive failure along pre-existing tectonic structures (e.g., Agliardi et al., 2001; Ustaszewski and Pfiffner, 2008; Arai and Chigira, 2019). The relationship between extensional tectonic structures and DSGSDs has been examined on Mt. Morrone in Central Apennines. Here, young normal faults in the lower part of the mountain front predisposes and trigger large-scale gravitational deformation, which is superimposed on older faults located at a higher elevation experiencing both tectonic and gravitational displacement (Gori et al., 2014).

This work analyses the tectonic geomorphology associated with the Acıgöl and Akgöl grabens in southwestern Türkiye, essentially by means of detailed mapping, field surveys and dating. The study is mainly focused on: (1) a peculiar array of intra-basin faults that have a significant geomorphic imprint in the southwestern sector of the Acıgöl Graben; and (2) the extensive occurrence of DSGSDs and large landslides in the fault-bounded uplifted carbonate range situated between the Acıgöl and Akgöl grabens. The scarcity of reports on DSGSDs in extensional terrains (e.g., fault-controlled range fronts) highlights the importance of identifying and differentiating gravitational and tectonic faults, especially in carbonate terrains where such gravitational slope failures are rare. The study area provides an ideal laboratory for studying these phenomena. To our knowledge, this work documents for the first time DSGSDs and a giant landslide (>1 Gm^3) in Türkiye. The main aspects addressed regarding the slope movements in an active extensional environment include: (1) potential preparatory and triggering factors; (2) passive and active role played by active faulting on the development of gravitational failures (favorable sliding planes, relief rejuvenation, debuttressing, seismic shaking); (3) evolutionary trends of DSGSDs and their transformation into large landslides; and (4) development of solution sinkholes in slopes affected by gravitational deformation.

2. General geological setting, neotectonics and seismic activity

The N*E*-SW trending Acıgöl Graben is one of the main morphostructures of the West Anatolian extensional province. This region lies in a backarc position with respect to the Aegean Arc, where the African plate subducts beneath the Eurasian plate. The ongoing extension in this intraplate region is primarily related to the southward displacement of the subduction zone (Le Pichon and Angelier, 1979; Reilinger et al., 2006) (Fig. 1A). The extensional province is characterized by a complex network E-W, NE-SW, and NW-SE trending neotectonic grabens. The Acıgöl Graben is located in the eastern part of this region, which also includes the NE-SW-trending Baklan and Burdur grabens and the NW-SE-oriented Dinar Graben (Fig. 1B). Additionally, the Akgöl Graben is a minor intermontane fault-angle depression located between the Acıgöl and Burdur grabens.

The geotectonic setting of western Anatolia is related to the development of the Alpine–Himalayan orogeny. The region contains two accreted microcontinents: the Pontides in the north and the Anatolid-Taurides in the south. The collision of these microcontinents during the early Tertiary, after the closure of the Neotethys Ocean, resulted in the formation of the İzmir-Ankara-Erzincan Suture (Şengör and Yılmaz, 1981; Okay and Tüysüz, 1999) (Fig. 1A). The timing and driving mechanism underlying the transition from contraction to extension within western Anatolia remain a subject of debate. Three primary models have been proposed to explain the extensional regime: (1) the orogenic collapse model, which suggests that extension in western Anatolia started in late Oligocene-early Miocene times due to spreading of the thickened crust, following the latest Palaeocene collision across the Neotethys (Seyitoğlu and Scott, 1991; Seyítoğlu and Scott, 1996); (2) the tectonic escape model, whereby the collision of the Anatolid-Taurides and Arabian plates along the Bitlis-Zagros Suture Zone in the middle Miocene was accompanied by the formation of the North Anatolian and East Anatolian strike-slip faults and the westward escape of the Anatolian plate, resulting in the development of grabens from the late Miocene (Dewey and Şengöl, 1979; Şengör et al., 1985; Şengör, 1987) (Fig. 1B); and (3) the back-arc spreading model, which explains the extension by trench rollback in the Aegean Arc and the S-SW migration of the subduction zone towards the subducting African plate (McKenzie, 1978; Le Pichon and Angelier, 1979; Meulenkamp et al., 1988) (Fig. 1B). However, the onset of the subduction (e.g., 26 Ma, 13 Ma, 5 Ma) and associated back-arc extension is a matter of debate (e.g., 12 Ma, 13 Ma, 5 Ma, >23 Ma; Meulenkamp et al., 1988, Le Pichon and Angelier, 1979; McKenzie, 1978; Thomson et al., 1998).

Based on basin stratigraphy, the formation of the NE-SW to ENE-WSW oriented Baklan, Acıgöl, and Burdur grabens began during the late Miocene (Sickenberg and Tobien, 1971; Şenel, 1997a; Göktaş et al., 1989; Alçiçek, 2009; Kazancı et al., 2012; Helvacı et al., 2013). While the age of the oldest sediments filling the Dinar and Akgöl grabens remains uncertain, Plio-Quaternary deposition has been reported in these basins (Koçyiğit and Gürboğa, 2010; Gürbüz et al., 2012; Alçiçek et al., 2013). Fault activity is evidenced by moderate to large historical and instrumental earthquakes (Fig. 1B). Seismic activity has been recorded in the Acıgöl Graben, which is controlled by the Acıgöl and Maymundağı faults along its southeastern and northwestern margins, respectively. A magnitude M_w 5.8 earthquake occurred on 08.08.2019 was attributed to the Acıgöl Fault (Sözbilir et al., 2019). Furthermore, paleoseismological studies have inferred three surface-rupturing earthquakes on the Acıgöl Fault, and at least five paleoearthquakes on the Maymundağı Fault (Kürçer et al., 2016; Özdemir et al., 2017). However, the geochronological data obtained to constrain the timing of the paleoearthquakes in the corresponding works are not published. On the Dinar Graben, a magnitude M_w 6.4 earthquake in 1995 (Kılıç et al., 2017) was accompanied by a surface rupture (Eyidoğan and Barka, 1996; Koral, 2000). Historical records from the ancient city Apamea Kibotos, situated on the northeastern margin of the Dinar Graben, report on three destructive earthquakes at 336–323 BCE, 88 BCE (I_o IX), and 54 CE (I_o VIII) (Başarır et al., 2017; Kadirioğlu et al., 2017). Trenching studies in the Dinar Graben further revealed evidence of paleoearthquakes dating back to 1500 BCE, 80 BCE, 111 BCE-916 CE, 916–1155 CE, and 1318–1428 CE (Altunel et al., 1999; Kürçer et al., 2021). The Burdur Graben also has a history of seismic events, including earthquakes in 1875 CE (I_o IX) and 1876 CE (I_o VI) (Başarır et al., 2017; Kadirioğlu et al., 2017). Notably, the 1914 earthquake (M_w 6.9) and the 1971 earthquake sequence (with a maximum M_w 5.9 event) (Kılıç et al., 2017), caused surface ruptures along the southeastern margin of the Burdur Graben (Taymaz and Price, 1992; Erinç et al., 1971). Additionally, earthquakes have been reported around the Baklan Graben, such as the 1875 CE (I_o IX), 1925 CE (M_w 6) and 1933 CE (M_s 5.7) events (Başarır et al., 2017; Kadirioğlu et al., 2017).

The Acıgöl Graben is superimposed on a strongly folded and fractured Jurassic-Cretaceous carbonate succession unconformably overlain by an Oligocene sedimentary sequence dominated by clastics (Fig. 2). The Akgöl Graben to the SE is superimposed on folded carbonate-dominated Mesozoic formations. These rocks belong to the Lycian Nappes consisting of rift and passive margin carbonate sediments, as well as Late Cretaceous ophiolite and mélange units (Collins and Robertson, 1998). A widely accepted hypothesis suggests that these tectonic units originated from the closure of the Pontides and the Anatolid-Taurides micro-continents and were subsequently transported

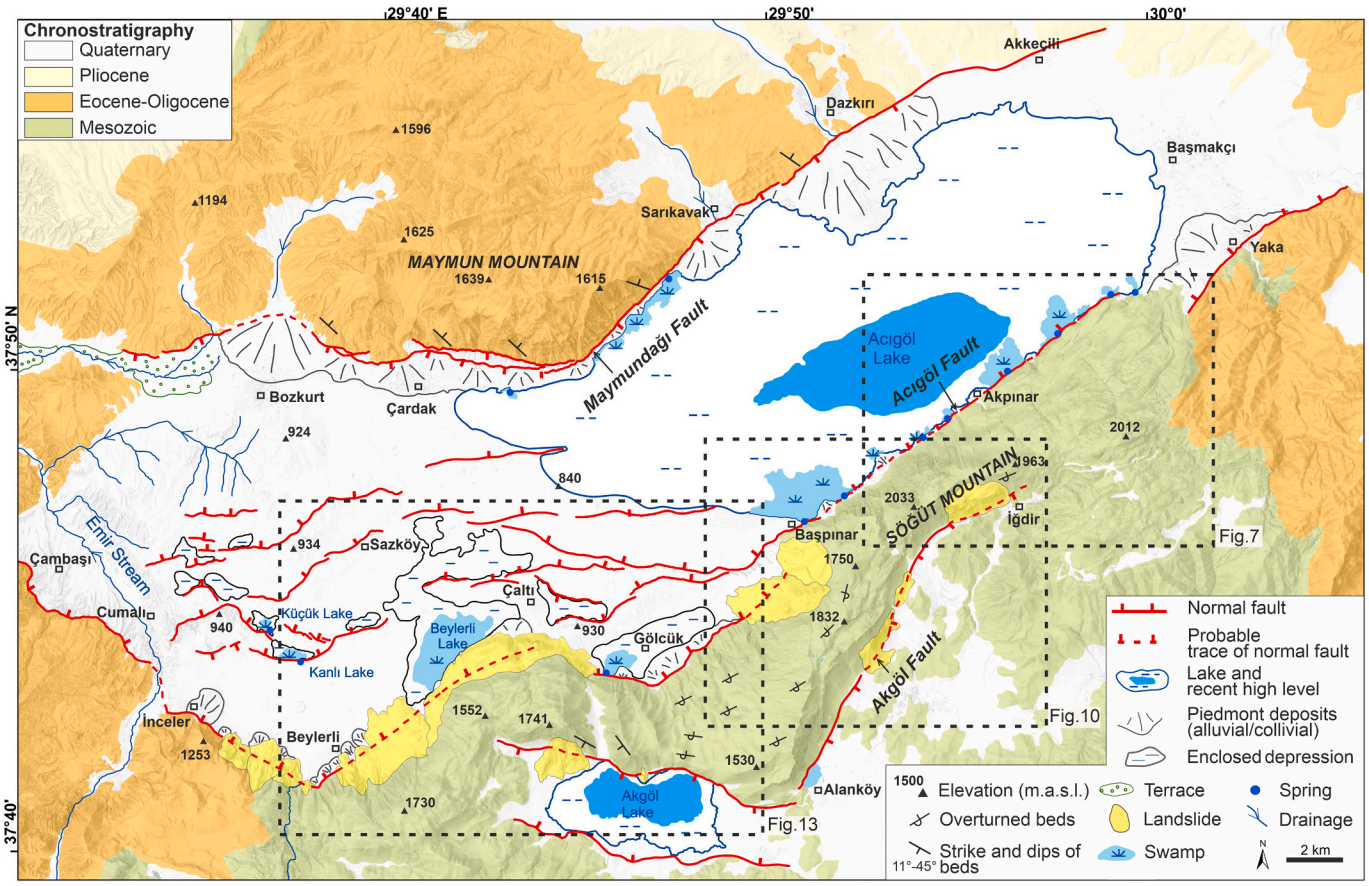

Fig. 2. Geological-gemorphological map of the Acıgöl and Akgöl grabens. Boxes show the location of Figs. 7, 10 and 13. Geology adapted from Şenel (1997a, 1997b).

southward (de Graciansky, 1972; Şengör and Yılmaz, 1981; Robertson and Dixon, 1984; Collins and Robertson, 1998). In the study area, the majority of the limestone outcrops occur in the uplifted block bounded by the Acıgöl and Akgöl faults (Fig. 2). The limestone units strike parallel to the range topography and display a general NW dip, locally with overturned attitude.

The exposed Oligocene sedimentary sequence shows a general NE dip and includes a wide variety of lithofacies deposited in various sedimentary environments, such as alluvial fans, fan-deltas, beaches, inner shelf carbonates and offshore deposits (Elmas et al., 2019). The debate about the onset of the extensional regime in the region is linked to the discussion on the tectono-sedimentary history of these deposits. According to the researchers who support a compressional regime during the Oligocene, the basin developed either as a molassic basin (Şengör and Yılmaz, 1981), or as a piggy-back basin association with the emplacement of the Lycian Nappes (Yilmaz et al., 2000; Gürer and Yılmaz, 2002). In contrast, according to those studies that contend extensional activity since the Oligocene, the sediments were deposited in a basin located between the Menderes Massif to the north and Lycian nappes to the south, and more specifically in the hanging wall of the Datça-Kale main breakaway fault, which exhumes the Menderes Massif as an asymmetric core complex (Seyitoğlu et al., 2004; Elmas et al., 2019). In alignment with this perspective, it is proposed that the Acıgöl Fault was a component of the Datça-Kale main breakaway fault during the Oligocene and controlled thickness variations in the Oligocene successions between the northwest (downthrown block) and southeast (upthrown block) block of this fault (Elmas et al., 2019). The region around the Acıgöl Graben has a semi-arid climate with a mean annual temperature of around 13 °C and 350–450 mm in average annual precipitation (Özdemir and Bahadır, 2009). The timberline is the region is situated around 2000 m a.s.l. (Kuzucuoğlu et al., 2019).

3. Methodology

This research is essentially based on geological-geomorphological mapping, field and drone surveys, and Optically Stimulated Luminescence (OSL) dating. Mapping involved the production of a geological-geomorphological map of the Acıgöl and Akgöl grabens, largely focused on Quaternary deposits and landforms to clarify active/recent tectonic faults. Three 1:5000 scale maps were produced mainly focused on slopes with DSGSDs to show the geomorphic expression of surface ruptures such as uphill facing scarp, linear depressions, and downhill-facing scarps. The maps were generated through the interpretation of various data sources, including: (1) orthoimages; (2) aerial photographs; (3) digital surface and relief models with a 5 m spatial resolution obtained from Turkish General Directorate of Mapping; and (4) 1:100,000 scale geological maps (Şenel, 1997a, 1997b). The preliminary maps were improved through detailed field surveys. Topographic surveys have been further developed by using drones and Structure from Motion Photogrammetry to obtain high-resolution images of some key areas and outcrops. In this study, tectonic fault refers to faults related to deviatoric regional stress fields, whereas gravitational fault refers to failures in slopes produced by gravitational deformation. A combined situation occurs when the shallow section of a tectonic fault experiences gravitational slip (e.g., Březný et al., 2018). Moreover, the term landslide is used as equivalent to slope movements (e.g., Cruden and Varnes, 1996), and thus is not restricted to mass movements with well-defined failure surfaces.

OSL samples were collected from deposits affected by tectonic faulting in the Acıgöl Graben, following the methodology described in Nelson et al. (2015). Samples for equivalent dose analysis were collected using a light-proof stainless steel tube, and a bulk sub-sediment sample for dose rate calculation was collected for each sampling point. The OSL

dating analyses were conducted at the Luminescence Dating Research Laboratory of the Institute of Nuclear Sciences at Ankara University, Türkiye, following the conventional luminescence dating laboratory procedures and protocols (e.g., Özpolat et al., 2021; Bayer Altın et al., 2021; Özpolat et al., 2022). Equivalent dose measurements were determined using a Single-Aliquot Regenerative-dose protocol (SAR) (Murray and Wintle, 2003). Cosmic dose rates were estimated from field information and geographical coordinates of the samples using Prescott and Hutton (1994) model. Total dose rate and ages were calculated using the online Dose Rate and Age Calculator for trapped charge dating (DRAC) and Luminescence Dose and Age Calculator (LDAC) (Durcan et al., 2015; Liang and Forman, 2019).

4. Geomorphology and geology of the Acıgöl and Akgöl grabens

The Acıgöl Graben is an internally drained basin around 50 km long and 15 km wide. On its northwestern margin, the 31 km long Maymundağı Fault defines the Maymundağı mountain front (Fig. 2). It extends for approximately 16 km from Dazkırı towards the southwest with a NE-SW orientation, and veers in a bend into an E-W trend extending along 15 km until Bozkurt. The southeastern margin of the graben is controlled by the 65 km long Acıgöl Fault, which defines the northern boundary of the Söğüt Mountains. This fault shows a relatively sharp bend that separates a 50 km long NE-SW section and a 15 km long section with NW-SE orientation (Fig. 2). The proximity of the Acıgöl Lake to the Acıgöl Fault, together with the higher elevation of the Söğüt Mountains, suggest an asymmetric graben structure with a more active southern side (Price and Scott, 1994). The Söğüt Mountains is a horst morphostructure bounded to the SE by the Akgöl Fault, which defines the northern edge of the Akgöl Graben (Fig. 2). The northeastern part the Akgöl Basin displays a half-graben structure, with its northwest margin controlled by a 12 km long NE-SW oriented section of the Akgöl Fault between Iğdir and Alanköy. The southwestern portion of the graben has a rather symmetric structure, bounded by an ESE-WNW trending section of the Akgöl Fault and an unnamed fault with similar trend on the opposite side. The Akgöl Lake is situated next to the northern margin of the graben, suggesting higher subsidence than in the opposite side of the basin. The crest of the Söğüt Mountains between the Acıgöl and Akgöl grabens is situated close to the latter graben, with a much steeper mountain front. The asymmetry of the Söğüt Mountains could be attributed to the comparatively more recent activity and/or higher slip rate on the Akgöl Fault.

Unlike the relatively straight trace of the mountain fronts associated with the Akgöl and Maymundağı faults, the mountain front-piedmont junction controlled by NW-dipping Acıgöl Fault along the southwestern edge of the Acıgöl Graben shows a more complex geometry, including step-overs, bends and curved sections with the convexity pointing towards the basin (Fig. 2). In the northeastern sector of the basin, around Başmakçı, an 8 km long section of the fault juxtaposes Oligocene conglomerates against Quaternary sediments. Towards the SW, after a 2 km wide step over, it displays a rectilinear fault trace along 16 km till Başpınar, juxtaposing Jurassic-Cretaceous limestones and Quaternary deposits. This section of the fault coincides with the maximum level of the present Acıgöl Lake and controls significant karst springs and swamps. Here, the mountain front is barely dissected by drainages and alluvial fans in the piedmont are almost lacking. Around Başpınar, the Acıgöl Fault splays into a number of E-W trending intra-basin faults with conspicuous geomorphic expression, forming a series of N-facing fault scarps and S-tilted surfaces (i.e., intrabasinal half-grabens). Beyond the splay around Başpınar, the Acıgöl Fault shows a left-stepping step-over. This fault section to the SW shows some bends and is largely concealed by landslide deposits (Fig. 2). The direction of the Acıgöl Fault abruptly changes from NE-SW to NW-SE around Beylerli. In this NW-SE-oriented section the fault juxtaposes Oligocene sediments against Quaternary deposits. The Emir Stream, a tributary of the Büyük Menderes River (Fig. 1B), crosses the Acıgöl Fault perpendicularly and bends in the basin to the NW running parallel to the fault (Fig. 2). The southwestern portion of the Acıgöl Graben has external drainage, whereas the remaining part functions as an endorheic basin.

In the southwestern part of the graben floor, >20 intra-basin fault scarps with a prevalent E-W orientation have been mapped (Fig. 3). Fault scarp lengths range between 300 m and 12 km and the majority face to the north. Additionally, the height of the scarps shows a general decrease towards the north, probably indicative of a chronological sequence, with younger faults towards the north. These intra-basin faults have compartmentalized the graben floor into a series of fault-angle depressions, resulting in enclosed fluvial-lacustrine sub-basins with longitudinal drainages (Fig. 3). The tilted blocks of these fault-angle depressions form south-sloping surfaces that control the position of the longitudinal drainages close to the faults. In this sector of the basin aggradation is essentially restricted to the troughs at the foot of the fault scarps, while the rest of the area, including the fault scarps and the tilted surfaces, are dominated by erosion. The configuration of the recent maximum levels of Acıgöl and Beylerli lakes is controlled by these intra-basin faults. At some road cuts, significant Quaternary deformation is observed within the basin sediments in the tilted blocks. For instance, beneath a 15 m high north-facing fault scarp east of the Kanlı Lake (Fig. 4), tabular fine-grained lake deposits and subrounded fluvial gravels are offset by two steeply dipping secondary faults with no geomorphic expression (Fig. 4B, C). Unfortunately, no correlative deposits have been found on both sides of the faults, indicating minimum throws of 11 m and 5 m for the southern and northern fault strands, respectively. Another noteworthy exposure reveals a 25-m long section of a tilted block to the east of Cumalı (Fig. 5A). In this section, secondary faulting with a distinctive horst and graben structure deforms tabular cemented gravelly and fine-grained sheetflood deposits (Fig. 5B). Throws of ca. 1.70 m and ca. 2.55 m can be measured on two faults with identifiable correlative beds on both sides of the ruptures. Despite the significant internal deformation, these faults lack any clear geomorphic expression, whereas the main intra-basin fault to the north has formed a conspicuous scarp.

The Gölcük swamp ('Gölcük' means small lake) occurs in an enclosed depression confined between the mountain front of the Acıgöl Fault and the S-tilted footwall surface of an intra-basin fault, which based on its height has vertically offset basin sediments at least 60 m (Figs. 3, 6). A transverse S-directed drainage pattern indicates the southward rotation of the surface. In the eastern sector of the rotated block, a well-exposed section exhibits thin-bedded lacustrine sand and clay with a progressive unconformity, with dips grading from 22° SW at the base to horizontal at the top. This growth stratal geometry reveals synsedimentary deformation controlled by the activity of the main basin-bounding fault. SW-dipping fan-delta sediments crop out in the western sector of the block. Two exposed beds at different stratigraphic levels were dated by OSL (Fig. 6). A sample from the base of the exposed tilted succession was dated at 24.8 ± 8.8 ka (Sample no: 18/08/21/2) (Fig. 6B) (Table 1). In the other outcrop, situated at a higher stratigraphic level, beds exhibit a gradual upward dip decrease (e.g., growth strata), ranging from 17 to 13° SE (Fig. 6C). The OSL sample from this location was dated at 24.1 ± 4.4 ka (Sample no: 18/08/21/1) (Table 1). These ages demonstrate that the basin-bounding and intra-basin faults have been active at least since the Late Pleistocene.

5. Deep-seated gravitational slope deformations

DSGSDs have been observed on the upthrown block bounded by the Acıgöl and Akgöl faults, which form the Söğüt Mountains dominated by Mesozoic carbonate rocks. The mountain range on the southeastern margin of the Acıgöl Graben, with a maximum local relief of around 1200 m, can be divided into three sectors, each exhibiting DSGSDs with distinct characteristics (Fig. 2): (1) Northeastern sector, associated with the northeastern portion of the Acıgöl Fault; (2) Central sector, where

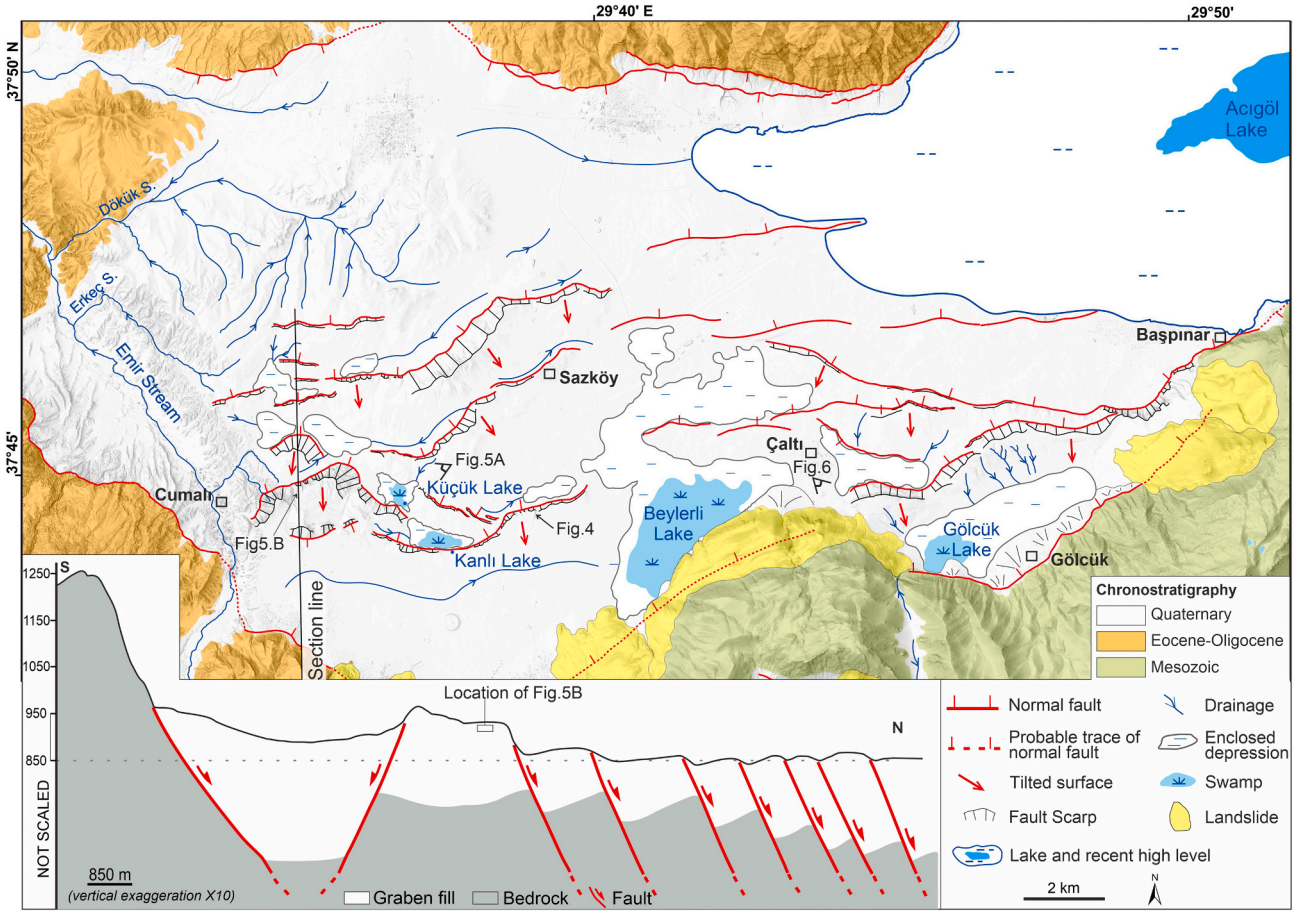

Fig. 3. Detailed geomorphological-geological map showing the intra-basin faults and associated morpho-structure in the southwestern part of the Acıgöl Graben. The trace of the cross-section is indicated on the map.

the range is bounded to the southeast by the Akgöl Fault, showing two steep and debuttressed fault-bounded flanks; and (3) Southwestern sector, where the trace of the Acıgöl Fault is largely concealed by landslide deposits and the southern slope of the range is bounded by the ESE-WNW section of the Akgöl Fault. Detailed maps of these sectors are provided in figures which location is shown in the general map of Fig. 2.

5.1. Northeastern sector

In this sector, the northwestern flank of the Söğüt Mountains associated with the Acıgöl Fault shows a series of uphill- and downhill-facing scarps (Fig. 7). Here, the range reaches a local relief of 1172 m, between 840 m and 2012 m a.s.l. The stepped and serrated slope profile displays two high-relief downhill-facing scarps, an upper and a lower one, as well as a steep basal slope associated with the Acıgöl Fault (Fig. 7). The upper downhill-facing scarp is associated with the crest of the range. This 480 m high scarp resembles the curved head scarp of a giant landslide with the concavity facing towards the basin. The lower downhill-facing scarp is situated around 2 km to the NW. This fresh-looking scarp reaches 300 m in height. Above this lower downhill-facing scarp there is a series of short and discontinuous linear depressions associated with uphill-facing scarps (Fig. 7, and inset section).

A total of 96 counterscarps have been mapped in the upper zone, with lengths ranging from 58 to 1166 m and an average of length of 327 m (standard deviation 234) (Fig. 7). These scarps are generally parallel to the topographic grain, and some exhibit a slight convexity towards the basin (Figs. 7, 8). The sediment-filled area of the linear depressions (flat bottom of the troughs) at the foot of the scarps vary from 313 m^2 to 35.139 m^2, with an average area of 5.758 m^2 (standard deviation 6.990 m^2). A significant proportion of the slope has internal drainage governed by the presence of numerous enclosed depressions associated with antislope scarps and a highly permeable fractured and karstified carbonate bedrock. Regarding the surface drainage, the longitudinal Cimcim Stream is controlled by the fault responsible for the upper downhill-facing scarp. In its upper reach, it flows towards the northeast like some of its tributaries at lower elevation adapted to linear troughs. The southwestern part of this northeastern sector is dissected by the transverse Cennet and Sunter streams. These NW-directed drainages locally exhibit sharp bends associated with troughs. Aside from these streams, the region remains largely devoid of gullies and a substantial portion of the surface water infiltrates into the rock massif, recharging the aquifer that discharges at numerous springs along the foot of the mountain front, feeding swamp environments (Fig. 7).

The upper zone is also characterized by the presence of solution sinkholes. A total of 66 sinkholes have been identified, locally forming alignments controlled by the gravitational features. A significant proportion of these sinkholes mainly correspond polygenetic depressions initiated by the creation of enclosed depressions by surface deformation and subsequently modified by enhanced dissolution at these sites with focused runoff and infiltration. Different geometries and distributions can be distinguished, including (1) Sinkholes associated with linear depressions, which can be further categorized as elongated or subcircular sinkholes. Elongated sinkholes may cover the entire trough area and they have been identified with an enclosed inward sloping. Subcircular sinkholes have a more circular geometry and are located at specific points within the troughs and (2) Sinkholes associated with uphill-facing scarp, characterized by subcircular shape in plan and developed on low-gradient surfaces next to uphill-facing scarps or along

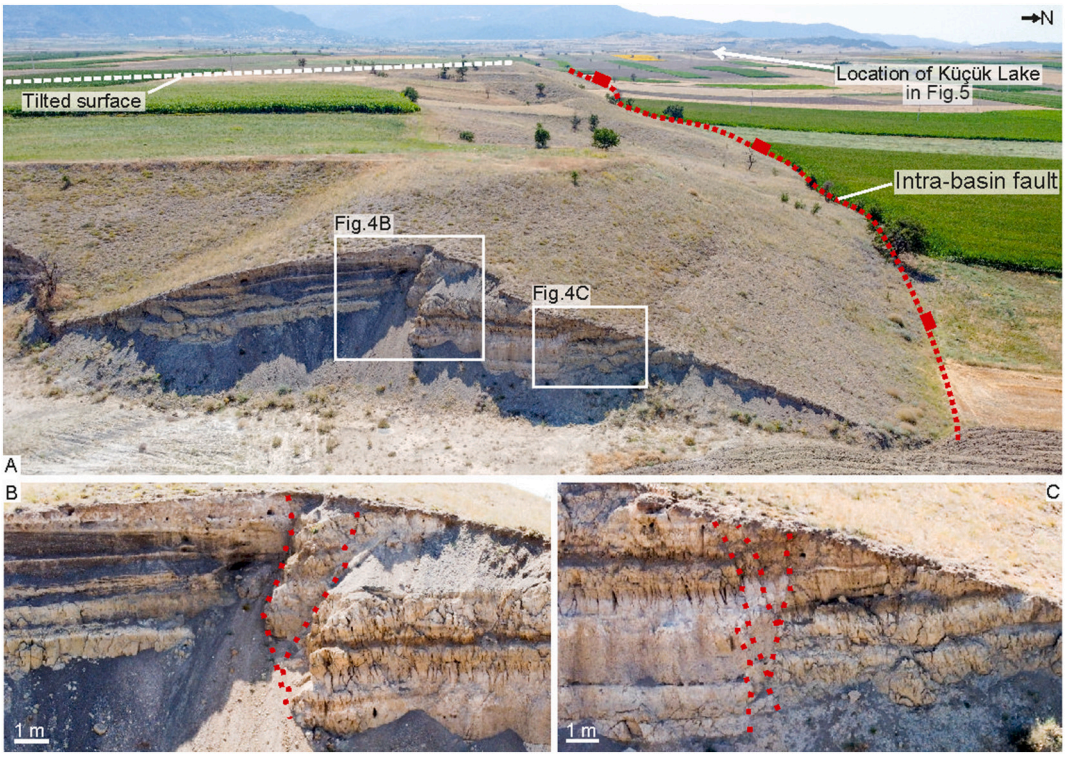

Fig. 4. A. Image of the intra-basin fault scarp located to the east of Kanlı Lake. Note the S-tilted surface of the footwall. B, C. Close-up views of secondary down-to-the-north normal faults. Note fault splay and oversteepening close to the surface in B and C. These normal faults refracted close to the surface due to low confining pressure, resembling reverse faults (pseudoreverse faults) in the upper part.

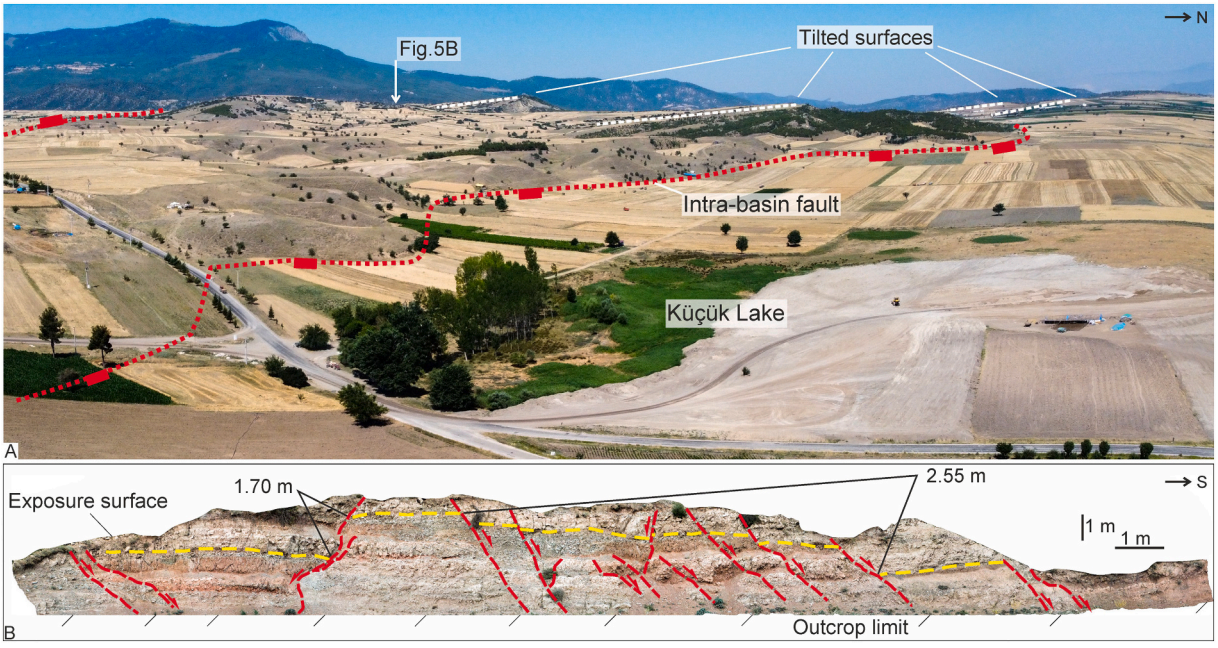

Fig. 5. A. Image of the intra-basin fault scarps and S-tilted surfaces in the southwestern part of the Acıgöl Graben. The Küçük Lake in the foreground exemplifies a closed depression formed on a downthrown block. The lake has been transformed into an ephemeral wetland altered by human activity. B. Road-cut exposure of basin sediments offset by normal faults in a titled block. The outcrop reveals a 25 m wide deformation zone with a horst and graben structure. See location of section in Figs. 3 and 5A. Note the different orientation of the upper and lower images.

their crest. In addition to these, two cover collapse sinkholes have been mapped in the trough deposits.

DSGSDs below the lower major downhill-facing scarp (lower zone) include uphill-facing scarps, downhill-facing scarps, and associated troughs (Fig. 8A, B). Two downhill-facing scarps are observed in this zone, one of which exhibits a cemented fault breccia. Within this zone, a total of 37 counterscarps have been mapped, ranging in length from 121 m to 1454 m, with an average value of 469 m (standard deviation 312).

Fig. 6. A. Image showing the intra-basin fault scarp in the southwestern part of the Acıgöl Graben. The red arrows point to the trace of the main fault along the mountain front, locally covered by landslide deposits. A red dashed line delineates the intra-basin fault that offsets the basin deposits. Location of the OSL samples is marked within the image. Inset sketch illustrates the relationship between the faults, the dated basin fill sediments with growth stratal geometries, landslide deposits at the basin margin and the carbonate bedrock. B. Image of the outcrop situated at the base of the intra-basin fault scarp. The southward dip is observed in the gravel deposits with intercalations fine-grained beds. **C.** Image of the outcrop situated at higher stratigraphic position with S-dipping gravel and sand beds.

Table 1
Data of the OSL analyses and estimated ages.

Sample number	Coordinates	Equivalent dose (Gy)	Cosmic dose (mGy/year)	Total dose (mGy/year)	Date (ka)	U (ppm)	Th (ppm)	K (%)	Rb (ppm)
18/08/21/1	37°44′12.08″ N/ 29°44′3.82″ E	58.93 ± 9.85	0.17 ± 0.02	2.46 ± 0.18	24.1 ± 4.4	11.7	0.6	0.25	0.5
18/08/21/2	37°44′31.41″N/ 29°44′23.82″ E	55.78 ± 18.8	0.2 ± 0.02	2.25 ± 0.16	24.8 ± 8.8	9.4	1	0.45	8.1

The sediment-filled area of the linear depressions ranges from 1.911 m^2 to 73.766 m^2, with an average area of 32.047 m^2 (standard deviation 24.559). In comparison, the average area of linear depressions is 5.6 times larger than the area of linear depressions in the upper zone. The lower depressions also have a clearer geomorphic expression, possibly indicative of a younger or more active development. Regarding the hydrology of this lower zone, many of the linear depressions are drained by drainages with sharp deflections.

In the northeastern part of the lower zone, fault breccias are exposed along some uphill-facing scarps (Fig. 8C, D). One of the fault planes which controls an uphill-facing scarp, striking N34E and dipping 69SE into the slope, displays slickensides (grooves, striations) indicative pure normal dip-slip displacement. Here, cemented fault breccia attached to the fault plane can be observed (Fig. 8E, F). In the southwestern part of the lower zone, the fault zone associated with an uphill-facing scarp has been exposed in a limestone quarry (Fig. 9A). The excavation shows: (1) a steep fault plane dipping into the slope (SE) strongly overprinted by karstification and secondary carbonate precipitation; (2) a cemented and karstified fault breccia made up of angular boulder- and cobble-sized clasts with grain supported texture (packbreccia) (Fig. 9B); and (3) a wedge-shaped deposit in the downthrown block consisting of massive residual clay (i.e., terra rossa derived from limestone dissolution) with scattered angular clasts (Fig. 9C).

5.2. Central sector

The central sector of the Söğüt Mountains is bounded by the Acıgöl Fault to the NW and the Akgöl Fault on the SE side and exhibits local reliefs of 900 m and 600 m, respectively (Fig. 10). West of the Efeklisivrisi Hill the range is dissected by NNW-SSE oriented valleys; the NNW-flowing Yenice Stream and the SSE-flowing Zeymenalanı Stream, both separated by an enclosed depression in the divide area, forming a saddle that resembles an old wind gap. To the NE of this saddle both sides of the range display conspicuous downhill-facing scarps. The arcuate downhill-facing scarp on the SE flank corresponds to the head scarp of a well-defined landslide, designated as LsC1. The head scarp of this landslide is around 150 m high and displays a clear concavity facing towards the Akgöl Basin. Lower part of the landslide mass has buried the Akgöl Fault (Fig. 10). The slid mass, approximately 1 km long and 2.3 km in wide, covers an area of 2.4 km^2. A volume of 324 Mm^3 has been roughly estimated assuming an ellipsoidal geometry for the failure plane. Uphill-facing scarps and troughs occur in the upper part of the landslide body with some elongated solution sinkholes. To the east of Nişantaşı Hill the upper part of the slopes displays downhill-facing scarps on both sides and a ridge-top depression in the intervening crestal area. This morpho-structure is 1200 m long and 200 m wide, and the elevation difference between the depression floor and the crest of the flanking scarps reaches 20 m. Five solution sinkholes occur within the depression, displaying elongated geometry in plan parallel to the trough's orientation (Fig. 11).

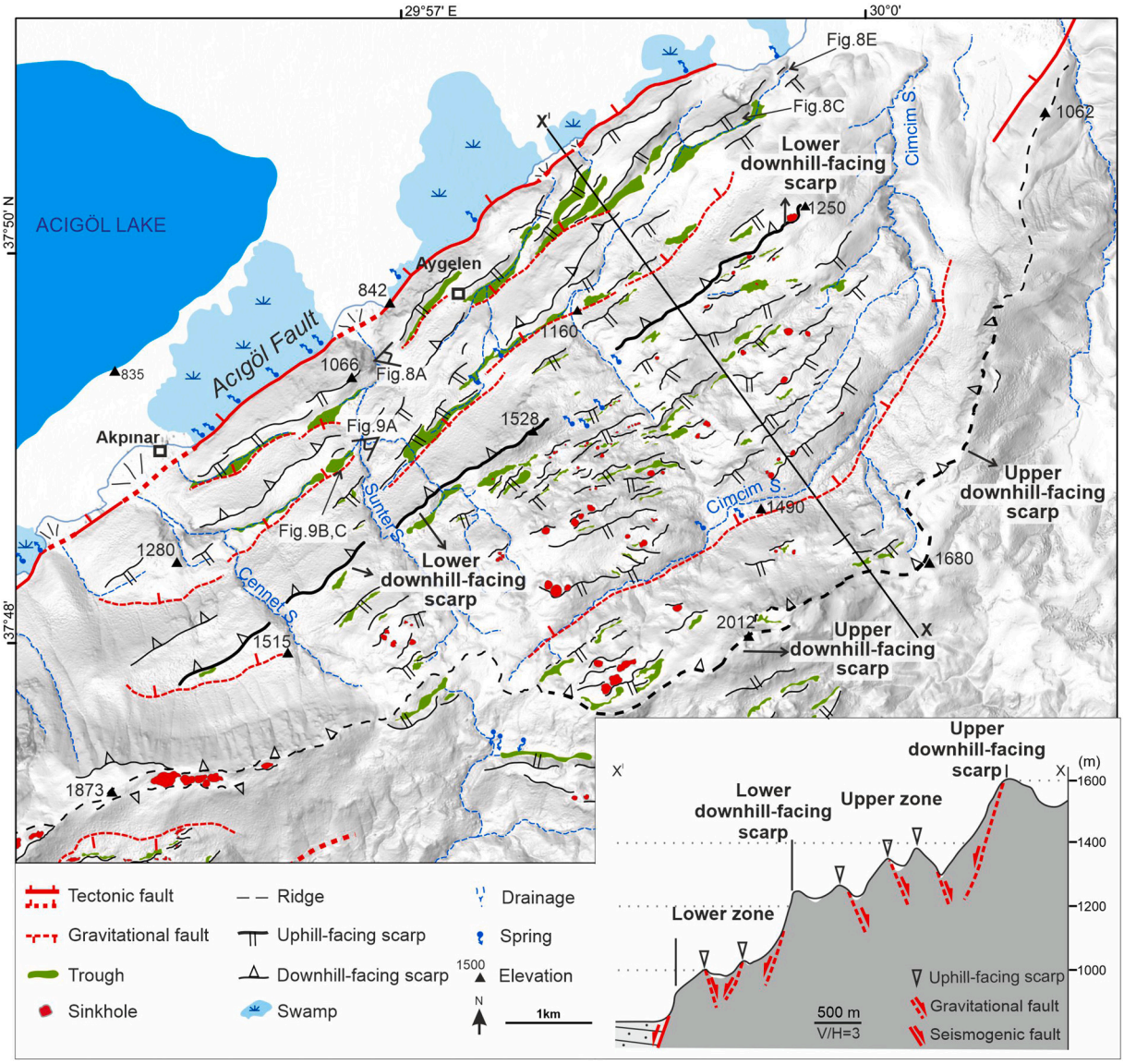

Fig. 7. Map depicting the DSGSDs in the northeastern sector of the Acıgöl uplifted block. The inset slope profile indicates the upper and lower zones bounded by major downhill-facing scarps.

Southwest of the Yenice and Zeymenalanı valleys the southeastern flank of the range shows vaguely defined evidence of lateral spreading including a gentle toe bulge that obscures the linear trace of the Akgöl Fault, while better-defined slope failures occur on the wider NW flank with greater local relief (Fig. 10). The upper part of the slopes on the SE side of the range displays two morpho-structural domains: (1) the northeastern portion with a serrated topography characterized by several uphill-facing scarp; and (2) the remaining southwestern portion that exhibits a ridge-top depression defined by a 2.5 km long uphill-facing scarp, which crest includes the Havna and Yüklü hills. In the former sector, the ridge crest is bounded by a *NE*-facing concave downhill-facing scarp and the uphill-facing scarps trend parallel to both the topographic and structural grain and some exhibit a slight convexity towards the basin (Fig. 12). In the latter portion, the ridge-top depression is drained longitudinally by the Zeladin Stream in the northeastern part. Further to the southwest the ridge-top depression splits into two troughs with closed depressions separated by an internal uphill-facing scarp. The floor on these twin depressions is clearly distinguishable by the presence of ephemeral lakes (Fig. 10 Inset section). The occurrence of linear enclosed depressions in the crestal zone indicate that the origin of the troughs is related to gravitational deformation rather than fluvial incision. Concerning the hydrology, the ridge is largely devoid of gullies, apart from the Zeladin Stream, suggesting that most of the runoff is interrupted by gravitational fault scarps and closed depressions and ultimately infiltrates into the pervious limestone bedrock. Solution sinkholes have been mapped either within the troughs or along the slopes associated with the uphill-facing scarps (Fig. 12B). Some of the sinkholes occupy the floor of the linear ridge-top depressions showing elongated shapes, characterized by elevation decrease towards their center. For instance, a large, elongated sinkhole has been mapped at the base of an uphill-facing scarp and ridge the forms Erikli Hill (Fig. 12B). A comparable elongated depression has been mapped in the southwestern part of the ridge-top depression hosting the ephemeral Kova Lake.

On the wider and higher-relief NW flank of the range the DSGSDs display a greater degree of development, with well-defined surface deformations extending all along the slope up to its foot (Fig. 10). The head of a DSGSD is defined by an upper curved downhill-facing scarp 200 m high with outward-facing concavity (Fig. 10). The upper part of the landslide mass is punctured by solution sinkholes. The lower arcuate downhill-facing scarps can be ascribed to two well-defined landslides:

Fig. 8. A. Uphill-facing scarps and linear depressions in the lower zone of the northeastern sector. The red dashed lines indicate uphill-facing scarps, white dashed lines represent troughs, and thin white dashed lines depict downhill-facing scarps B. Northeastern sector of the lower slope. Its location is indicated in A. C. Close-up image of the uphill-facing scarp shown in B. D. Fault breccia observed along the scarp in C. E. Close-up image of the uphill-facing scarp and exhumed fault plane with a strike and dip measurement of N34E and 69° SE. F. Close-up image of the fault breccia associated with the normal fault shown in E. The hammer rests on cemented breccia juxtaposed against the fault plane.

LsC2 and LsC3. The landslide LsC2 has a convex head scarp over 200 m high. The foot of this landslide scarp has guided the path of a stream in its southwestern part, while clusters of solution sinkholes occur in its eastern part. The backtilted head of the slid mass suggests rotation over a listric sliding plane (Fig. 10, inset profile). This landslide is 1.8 km long and 2.2 km wide and covers an area of 4.6 km^2. A volume of 575 Mm^3 has been estimated. The 300 m high head scar of landslide LsC3 cuts landslide LsC2 and displays a conspicuous depression at its foot. This depression, bounded with an uphill-facing scarp on the downslope side, could be attributed to the formation of an intra-landslide keystone graben, controlled by the main sliding surface with listric geometry and a secondary antithetic fault. The displaced mass is 2.3 km long, 1.5 km wide and covers an area of 2.7 km^2. Its volume has been roughly estimated at 160 Mm^3, considering an ellipsoidal geometry for the failure surface. The landslide masses of both LsC2 and LsC3 have buried the basin-bounding fault in a step-over zone.

Fig. 9. A. Uphill-facing scarps and associated linear depressions in the lower zone of the northeastern sector. The red dashed line indicates the trace of the Acıgöl Fault at the foot of the mountain front, white dashed lines represent linear depressions, and thin white dashed lines depict downhill-facing scarps. The location of the quarry shown in B and C is indicated. B. Highly brecciated bedrock exposed on the upthrown side of the fault scarp. The red circle indicates a person for scale. C. Fault controls the uphill-facing scarp and wedge-shaped deposits juxtaposed to the fault consist of massive residual clay with angular locally derived limestone clasts. On the upthrown side, fractures and brecciated bedrock exposure reveals discontinuity planes widened by dissolution in the epikarst zone.

5.3. Southwestern sector

DSGSDs are conspicuous in the southwestern sector of the Söğüt Mountains, south of Çaltı village (Fig. 13). This part of the mountain displays an asymmetric topographic profile, characterized by a steep southern flank and a gentler northern side with serrated morphology. The Acıgöl Fault at the foot of the northern slope shows a sharp bend with the convexity pointing towards the basin and is largely buried by landslide deposits (LsW2). The southern slope is bounded by an ESE-WNW-oriented section of the Akgöl Fault, which is partly concealed by a landslide (LsSW1). The local relief is higher on the northern slope extensively modified by gravitational deformation (850 m versus 710 m). Bedrock in these landslide areas is strongly fractured and brecciated, so that bedding has been largely obliterated by gravitational deformation. The eastern boundary of the sector affected by DSGSDs is defined by two deeply entrenched valleys flowing towards the Akgöl and Acıgöl basins, which might correspond to an abandoned uplifted valley (i.e., wind gap) (Fig. 14).

The lower portion of the northern slope exhibits a prominent downhill-facing scarp ascribable to the head scarp of a laterally continuous landslide complex (LsSW2) that buries the Acıgöl Fault. The 300 m high head scarp of the landslide complex shows a broad convex trace coherent with the bend of the Acıgöl Fault, changing from NW-SE direction in its eastern sector to E-W, and eventually curving towards the NE-SW in the western sector. In the northeastern sector the lower part of the landslide mass displays a conspicuous 6 km wide bulge and a marked convexity in plan, penetrating into the basin (Fig. 14). In the southwestern sector, the upper edge of the slid body is marked by a sharp slope break and the sharp interruption of the drainage net carved in the head scar. The landslide complex is 2.3 km long, 12 km wide and covers an area of 14.2 km^2. A volume of 3500 Mm^3 has been roughly estimated assuming an elliptical failure surface. The eastern part of the landslide complex overlies basin sediments on the upthrown block of an intra-basin fault, equivalent to those dated by OSL further to the east at 24.1 ± 4.4 ka and 24.8 ± 8.8 ka. This suggests a maximum age of 24 ka for this part of the landslide complex (see detailed explanation in Section 3).

On the northern slope, a total of 18 counterscarps scarps have been mapped, with lengths ranging from 85 and 1327 m and an average of length of 563 m (standard deviation 339) (Fig. 13). These scarps exhibit a consistent alignment with the topographic grain of the area, and some of them display a subtle convexity towards the basin. Linear depressions are observed at the foot of the uphill-facing scarps and above the landslide scarp (Fig. 13). Moreover, two elongated solution sinkholes superimposed on sackung troughs have been mapped in the upper part of the slope, close to the crestal area.

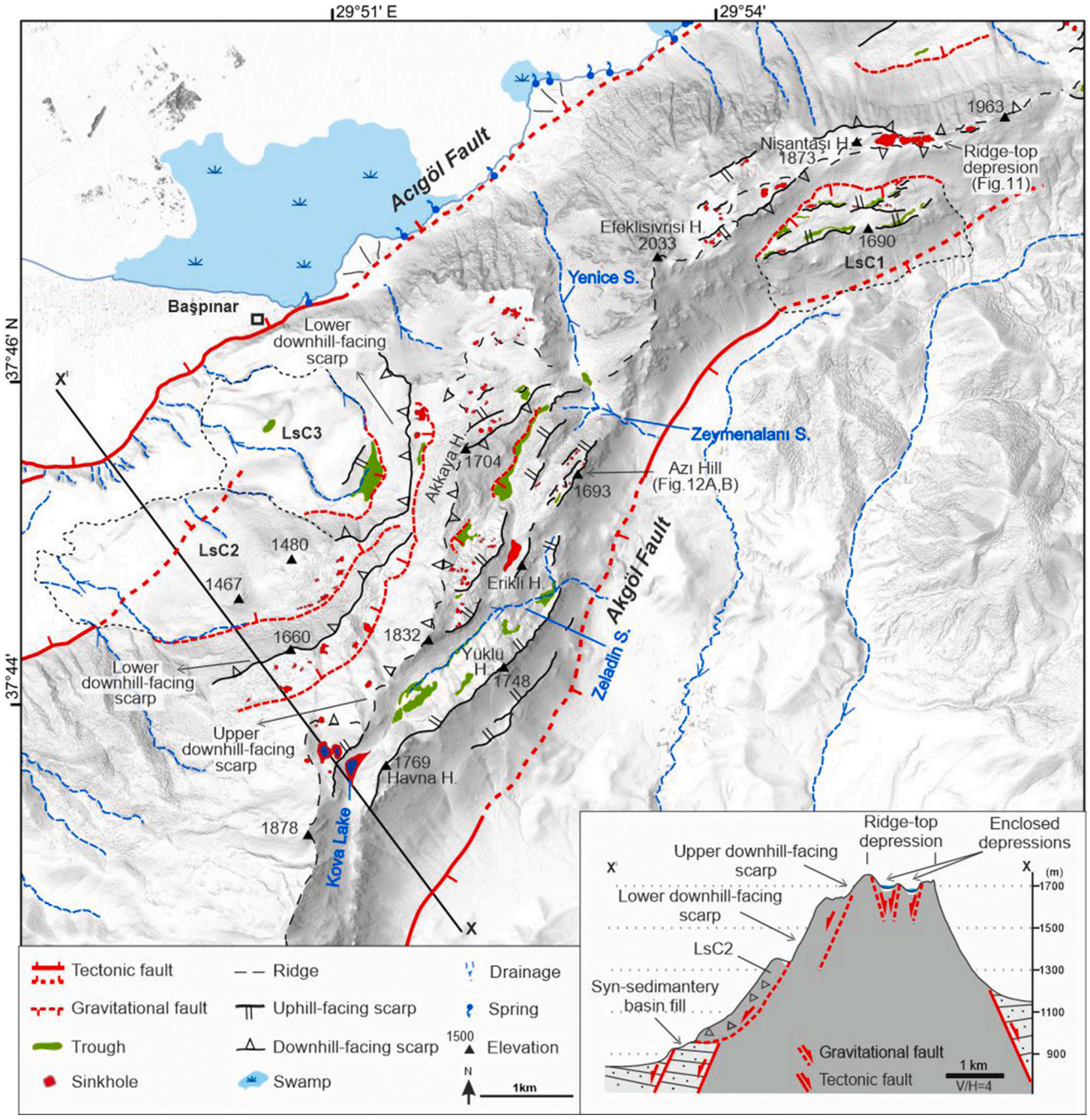

Fig. 10. Map illustrating the DSGSDs in the central sector of the fault-bounded Söğüt Mountains.

Regarding the hydrology of the slope, the thoroughgoing and N-flowing Ayı Stream shows sections influenced by troughs and scarps, including knick points. Additionally, an anomalous SW-directed drainage pattern is evident along the foot of the downhill-facing scarp. Except from these streams, the region remains largely devoid of gullies and a significant portion of the surface water infiltrates. The groundwater most probably discharges at the foot of the mountain front feeding Beylerli Lake. However, the location of the karst springs remains obscured, likely due to the northward displacement of the gravitational slope deformation.

Road cuts along the eastern boundary of landslide LsSW2 expose Quaternary deformation structures. One of the sections located in the lower part of the slope shows a prominent fault that juxtaposes a broad and compact fault breccia in the upthrown block against coarse-grained colluvial deposits in the downthrown block, which is in turn underlain by a landslide mass disintegrated into a dilated bouldery breccia. This fault, oriented N95E with a dip angle of 65° towards the north, exhibit dip-slip displacement as indicated by striations (with a rake of 80NE) (Fig. 15). To the north of the failure zone, within the downthrown block, the bedding of the angular gravel deposits shows a noticeable dip increase towards the bedrock, attributable to fault dragging (Fig. 15A). In the upthrown block to the south of the fault, steeply dipping faults and shear zones aligned with the main fault are apparent in the brecciated bedrock. Cartographic and geometrical relationships indicate that the exposed fault corresponds to one of the strands of the Acıgöl Fault and it likely controlled the upper edge of landslide LsSW2. It has also offset the post-24 ka landslide LsSW2 plus the overlying colluvial deposits of probable Holocene age.

Approximately 450 m south of the fault exposure, road cuts along the eastern and western side of the valley provide evidence of recent

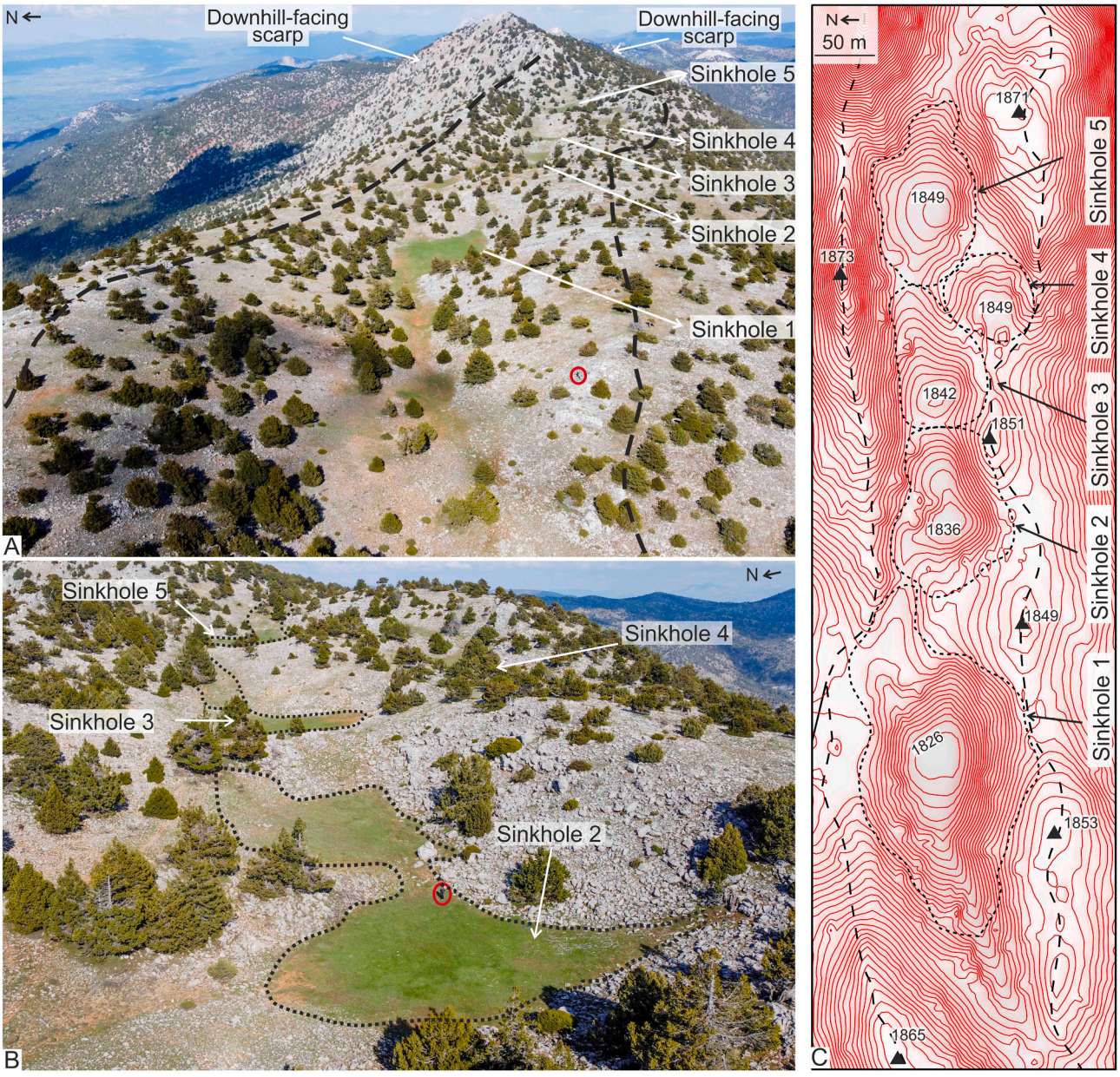

Fig. 11. A. Image of the ridge-top depression east of the Nisantaşı Hill bounded by downhill-facing scarps. Solution sinkholes within the depression are numbered from west to east. Red circle indicates person for scale B. A closer perspective of sinkholes 2, 3, 4, and 5 shown in Fig. A. Black dashed lines delineate the edge of the sinkhole floors. Red circle indicates person for scale. C. Topographic map with 1 m contour interval displaying the sinkholes illustrated in A and B. Thick dashed lines mark the divides of the ridge-top depression and while thin dashed lines the sinkhole edges.

deformation associated with an uphill-facing scarp (Fig. 14). In the eastern section, the fault plane of the uphill-facing scarp, striking N58W and dipping 68 SW, juxtapose angular colluvial deposits (i.e., talus) with bedrock (Fig. 16A, B). In the western section, the main fault is concealed and bounds to the north alluvial fan deposits. However, the alluvial succession displays a S-facing monocline attributable to drape folding above a blind S-dipping secondary normal fault (Fig. 16C).

6. Discussion

6.1. Tectonic Geomorphology

The Acıgöl Graben displays a marked asymmetry partially related to the different nature of the bedrock on both margins (Fig. 2). The northwestern margin is underlain by detrital Paleogene rocks carved by densely dissected drainage basins, which trunk channels feed large alluvial fans in the piedmont. Here, the dissected mountain front displays well-developed compound triangular fault facets. In contrast, the southeastern margin, dominated by Mesozoic carbonate rocks, shows very limited fluvial incision. The mountain front escarpment on carbonate bedrock is barely dissected and thus alluvial fans are scarce and display limited development. The restricted dissection and surface runoff on this margin of the basin can be attributed to three main factors: (1) high permeability of the bedrock, in which dissolution is favored by intense tectonic and gravitational fracturing; (2) development of gravitational surface ruptures such as antislope scarps that contribute to increase infiltration by blocking surface runoff; and (3) the development of solution sinkholes, often associated with topographic lows created by surface deformation. The southeastern margin is dominated by an internal karst drainage. An implication derived from the restricted surface

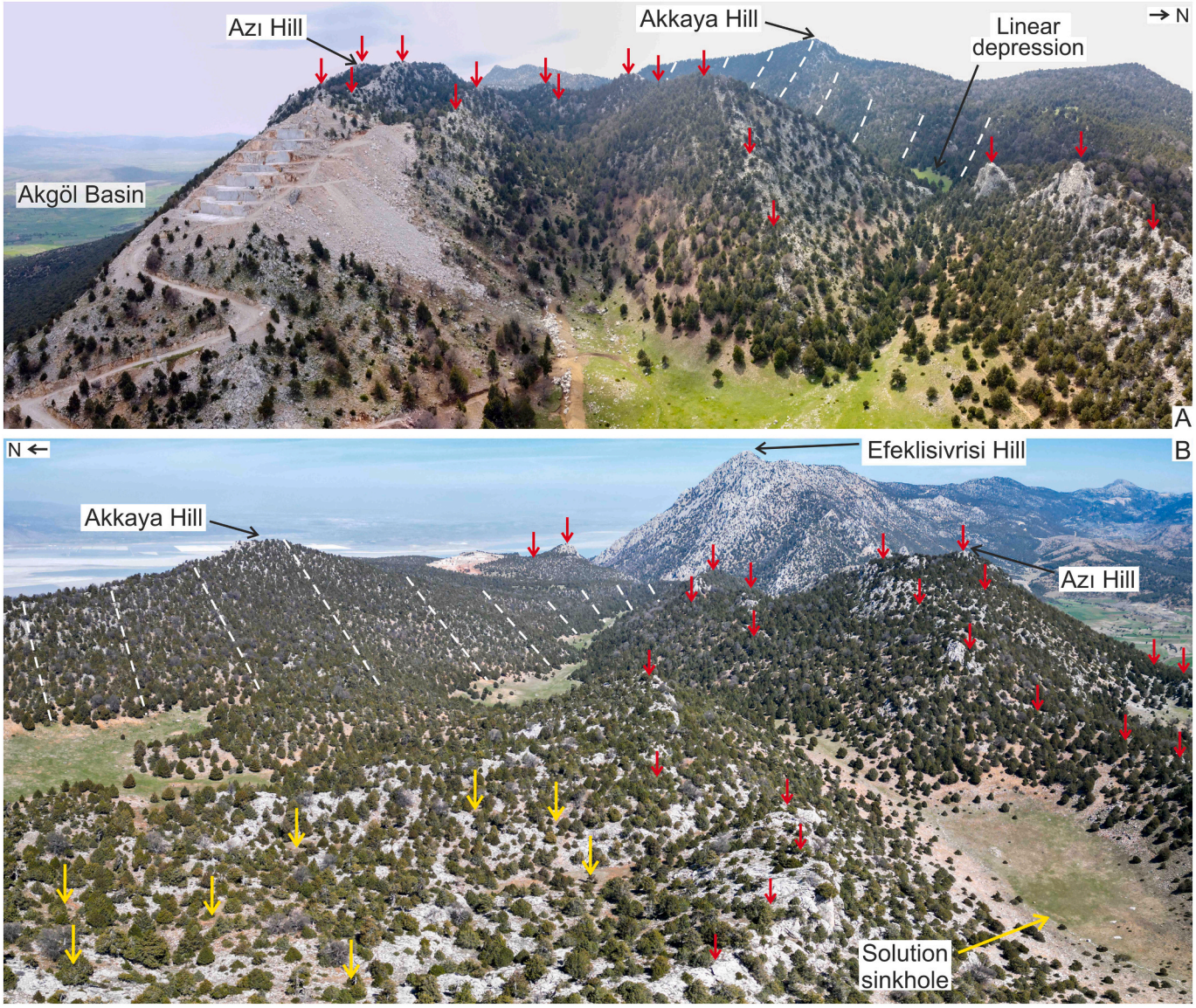

Fig. 12. A. Image showing the serrated topography southwest of Yenice and Zeymenalanı valleys. Note the multiple parallel uphill-facing scarps and troughs within this area. The SE-facing downhill-facing scarp is highlighted by dashed white lines. The crest of uphill-facing scarps is indicated by red arrows. B. The same serrated topography as in image A but taken looking to the NE. Solution sinkholes are visible in the limestone outcrops between the two large depressions (indicated by the yellow arrow). Additionally, a large, elongated solution sinkhole is superimposed on the linear ridge-top depression on the lower-right corner.

runoff and fluvial incision is the very limited sediment supply to the basin and low aggradation rate. This may explain the presence of a swarm of intra-basin half grabens with conspicuous geomorphic expression in the southwestern sector of the graben floor, which behaves as a starved basin where surface deformation overwhelms aggradation (Fig. 3). The limited geochronological data available (OSL ages) from basin sediments offset by intra-basin faults indicate that these structures have been active in late Quaternary times (<24 ka). Nonetheless, the fault scarps on easily erodible sediments and the impact on the drainage (e.g., strike streams, lakes) support current fault activity with significant slip rates. The geomorphic imprint of the intra-basin faults increases towards the basin axis, which may reflect a chronological sequence, variable slip rates, and/or a basinward decrease in the aggradation rate. A number of authors document basinward migration of faulting in grabens of the Basin and Range (USA) and central Greece (Leeder and Jackson, 1993; Jackson, 1999). Better understanding of the history of intra-basin faults (i.e., initiation, propagation, linkage) from active examples with geomorphic expression such as those of the Acıgöl Graben can provide valuable insights into the evolution of *syn*-rift depocenters and basin architecture (e.g., Northern North Sea, Dawers and Underhill, 2000; Suez Rift, Sharp et al., 2000), with implications for the exploration and development of hydrocarbon reservoirs (e.g., Leeder and Gawthorpe, 1987; Jackson and White, 1989; Prosser, 1993; Gawthorpe and Leeder, 2000; Gawthorpe et al., 2003; Demircioğlu et al., 2010; Rees et al., 2014; Cowie et al., 2000).

Field observations and modelling shows that basin-bounding normal faults evolve through growth, interaction, and linkage of initial arrays of isolated faults (Anders and Schlische, 1994; Cowie, 1998a; Gupta and Scholz, 2000). These processes influence the geomorphic and tectono-sedimentary evolution of basins based on two fundamental patterns: (1) uneven displacement along faults, with the highest throw at the center, decreasing towards the tips; and (2) scaling between fault length and maximum displacement, whereby longer faults display higher displacement (Cowie and Scholz, 1992; Cowie et al., 2000). At the early stages extensional systems are typically characterized by numerous small faults that accommodate distributed displacement, resulting in

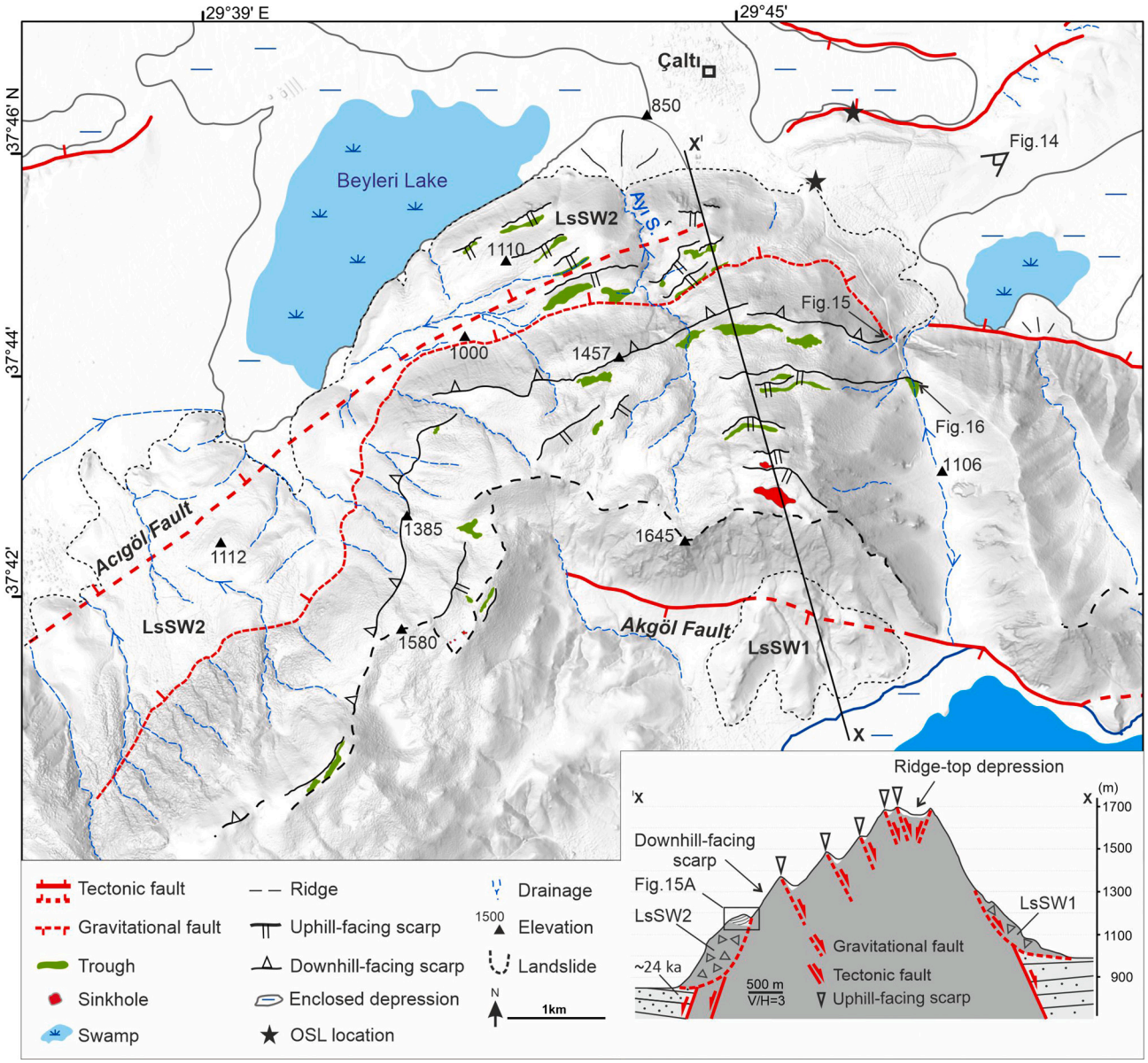

Fig. 13. Map illustrating the DSGSDs in the southwestern sector of the Söğüt Mountains. Inset cross-section shows sackung scarps and landslides.

small shallow fault-bounded depressions (Cowie et al., 2000; Gawthorpe and Leeder, 2000). As the faults propagate towards the tips of other nearby faults, interaction between nearby faults occurs, leading to direct linkage (Cowie, 1998b) or the development of accommodation ramps that eventually rupture (soft to hard linkage) (McGill and Stromquist, 1979; Walsh and Watterson, 1988; Cartwright et al., 1995; Trudgill, 2002). Eventually, linkage results in longer faults with higher displacement in the central section (Gupta and Scholz, 2000). The SW sector of the Acıgöl Basin represents a good example of the tectonic geomorphology associated with a complex intra-basin fault array accommodating distributed displacement. The conspicuous geomorphic expression of the fault array within a context of low aggradation rate provides insight into the landscape evolution governed by normal faulting, which ultimately controls the stratigraphic and structural features of grabens. This case study provides a field example that illustrates the evolution of a fault array with different displacement patterns, substantiating concepts based mainly on modelling studies (e.g., Cowie et al., 2000).

6.2. *Factors controlling slope instability*

Detailed mapping of the uplifted block on the southeastern margin of the Acıgöl Graben (Söğüt Mountains) bounded by the active Acıgöl and Akgöl faults, reveals the presence of extensive DSGSDs and large, short-runout landslides in carbonate bedrock. Factors controlling slope instability can be grouped into predisposing, preparatory, triggering, and sustaining factors (Glade and Crozier, 2005). Predisposing factors represent static factors that influence the inherent susceptibility of slopes to instability, and that may amplify the effect of other dynamic instability factors. The main predisposing factors involved in the analyzed area include: (1) the high relief and gradient of the slopes created by normal faulting; (2) the presence of laterally unconfined rock masses in slopes with convex geometry in plan, associated with sharp fault bends and stepovers (central and southwestern sectors; Figs. 10, 13); and (3) intense fracturing of the bedrock related to both paleotectonic and neotectonic deformation. Numerous studies illustrate that the anisotropy of rocks related to the presence of discontinuity planes such as bedding planes, joints and faults plays a significant role in reducing rock strength on high relief-slopes, and influences the size, geometry,

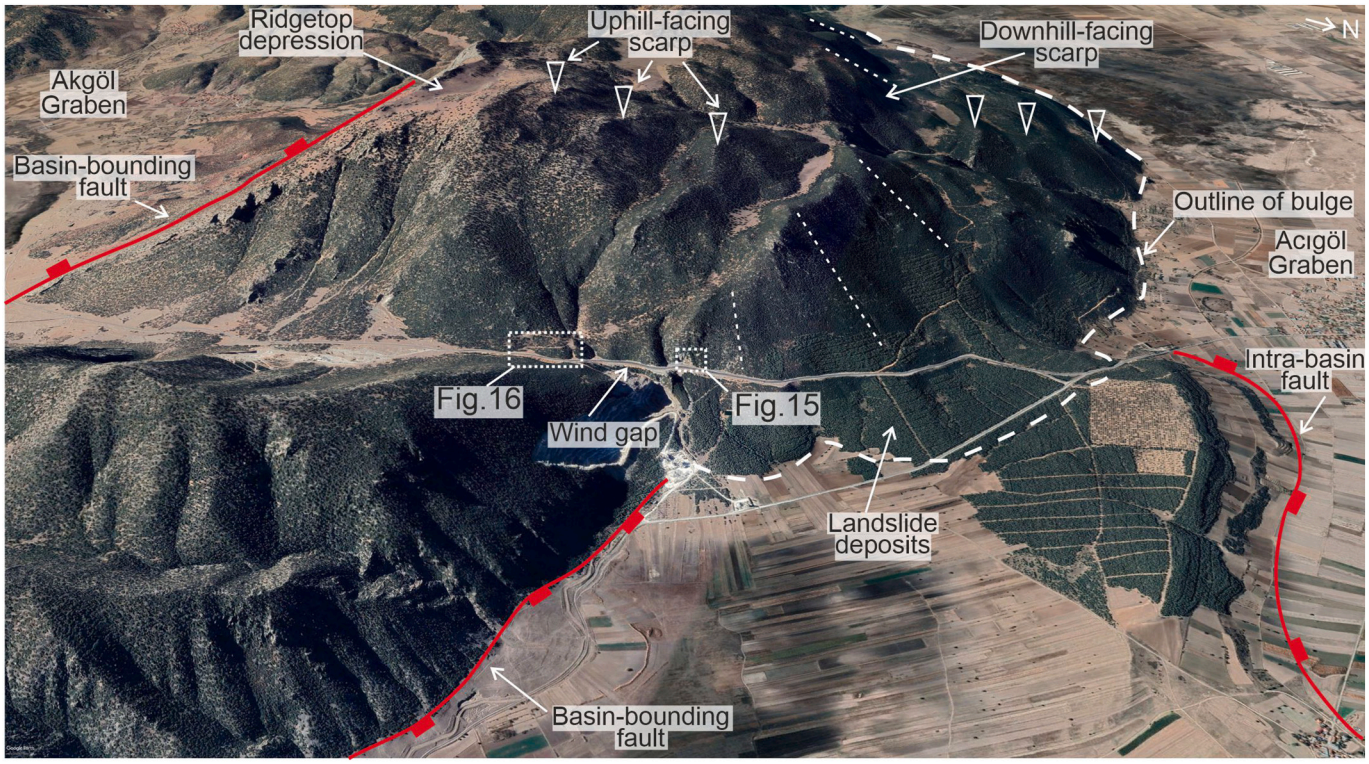

Fig. 14. Images captured from Google Earth (2023 CNES/Airbus) illustrating DSGSDs and faults in the southwestern sector of the Söğüt Mountains. Location of Figs. 15 and 16 indicated.

and failure mode of DSGSDs (McCalpin and Irvine, 1995; Agliardi et al., 2001; Di Luzio et al., 2004; Ambrosi and Crosta, 2006; Pánek et al., 2011). In the study area, the bedrock in broad zones associated with the basin bounding faults shows very intense fracturing, often making impossible to identify traces of bedding.

Preparatory factors are dynamic controls that contribute to reduce stability over time, without directly initiating the movement. In contrast, triggering factors cause a change in the condition of the slope from marginally unstable to unstable, leading to the onset of movement (Glade and Crozier, 2005). In most cases, the triggers correspond to an external force such as seismic shaking or heavy rainfall, but movement initiation may be also related to non-external processes such as weathering or rock mass creep that progressively reduce rock mass strength (e.g., Delchiaro et al., 2019). Preparatory factors have a dynamic nature and can evolve into triggering factors. A number of factors may have been preparatory for the documented DSGSDs include; (1) creation of high-relief slopes by uplift (e.g., Dramis and Sorriso-Valvo, 1994; Galadini, 2006); (2) coseismic ground motion, which can be affected by topographic amplification (constructive interference of seismic waves), causing cyclic changes in the stresses and reducing rock mass strength (e.g., Di Luzio et al., 2004; Agliardi et al., 2009; Hovius et al., 2012; Kaneda and Kono, 2017); (3) loss of basal support related to subsurface dissolution of evaporite or carbonate rocks (e.g., Maffei et al., 2005; Pánek et al., 2009; Discenza et al., 2011; Gutiérrez et al., 2012a, 2023). In the Söğüt Mountains, rock uplift related to ongoing activity on the Acıgöl and Akgöl faults results in a long-term process of relief rejuvenation, involving an increase in the height of the slopes and debutressing of new rock mass progressively brought to the surface in the footwall by normal faulting (Fig. 17). Moreover, large earthquakes sourced from these faults and other nearby seismogenic faults may contribute to rock mass weakening. Karstification of carbonate rocks is often considered to play a significant role in rock mass weakening. However, this process most probably has a limited impact in the development of the investigated DSGSDs, since carbonate dissolution mostly occurs in the upper few meters beneath the surface (epikarst; Fig. 9), where infiltration water losses great part of its dissolution capability (Palmer, 1991; De Waele and Gutiérrez, 2022). In contrast, deep-seated dissolution can play a significant preparatory role in evaporite karst areas (see review in Gutiérrez et al., 2023).

Defining the triggering factors for past displacement on a given DSGSD is not always straightforward due to a variety of factors: (1) it can be very challenging to demonstrate the contemporaneity between a potential trigger (e.g., paleoearthquake) and the onset of movement because of the lack of geochronological data, or insufficient temporal resolution and accuracy of the datings (e.g., McCalpin and Hart, 2002); and (2) some DSGSDs show an episodic kinematic style (Gutiérrez et al., 2008; McCalpin and Hart, 2002; McCalpin and Jones, 2021) and displacement events may be triggered by different factors (e.g., Livio et al., 2022). In an exceptional case study, Komura et al. (2020), based on a comprehensive trenching and geochronological investigation, found consistency between surface-rupturing paleoearthquakes on the Neodani strike-slip fault in central Japan and four displacement events in a nearby DSGSD. Studies on currently active DSGSDs demonstrate the causal link between slope deformation and historical seismic activity (e.g., Cotton et al., 1989; Jibson et al., 2004; Moro et al., 2007; McCalpin and Corominas, 2019). Seismic triggering can be related to earthquakes sourced from slope-bounding active faults in mountain fronts (e.g., Moro et al., 2007), or nearby faults, as evidenced by historical reactivation of fault scarps in a ridge-top depression in the Stillwater Range during the 1915 Pleasant Valley earthquake (Mw 7.3) and the 1954 Dixie Valley-Fairview Peak earthquakes (Mw 6.8 and 7.2), with epicenters about 30 km north and 7 km south from the depression, respectively (McCalpin and Jones, 2021). Large earthquakes sourced from the 65 km long Acıgöl Fault and the 22 km long Akgöl Fault are likely the most significant triggers for the studied DSGSDs and landslides. Additionally, the Maymundağı Fault at the northwestern margin of the Acıgöl Graben, and other nearby basin-bounding faults (SW margin of Akgöl Graben, NW margin of Burdur Graben; Fig. 1B) can generate morphogenetic

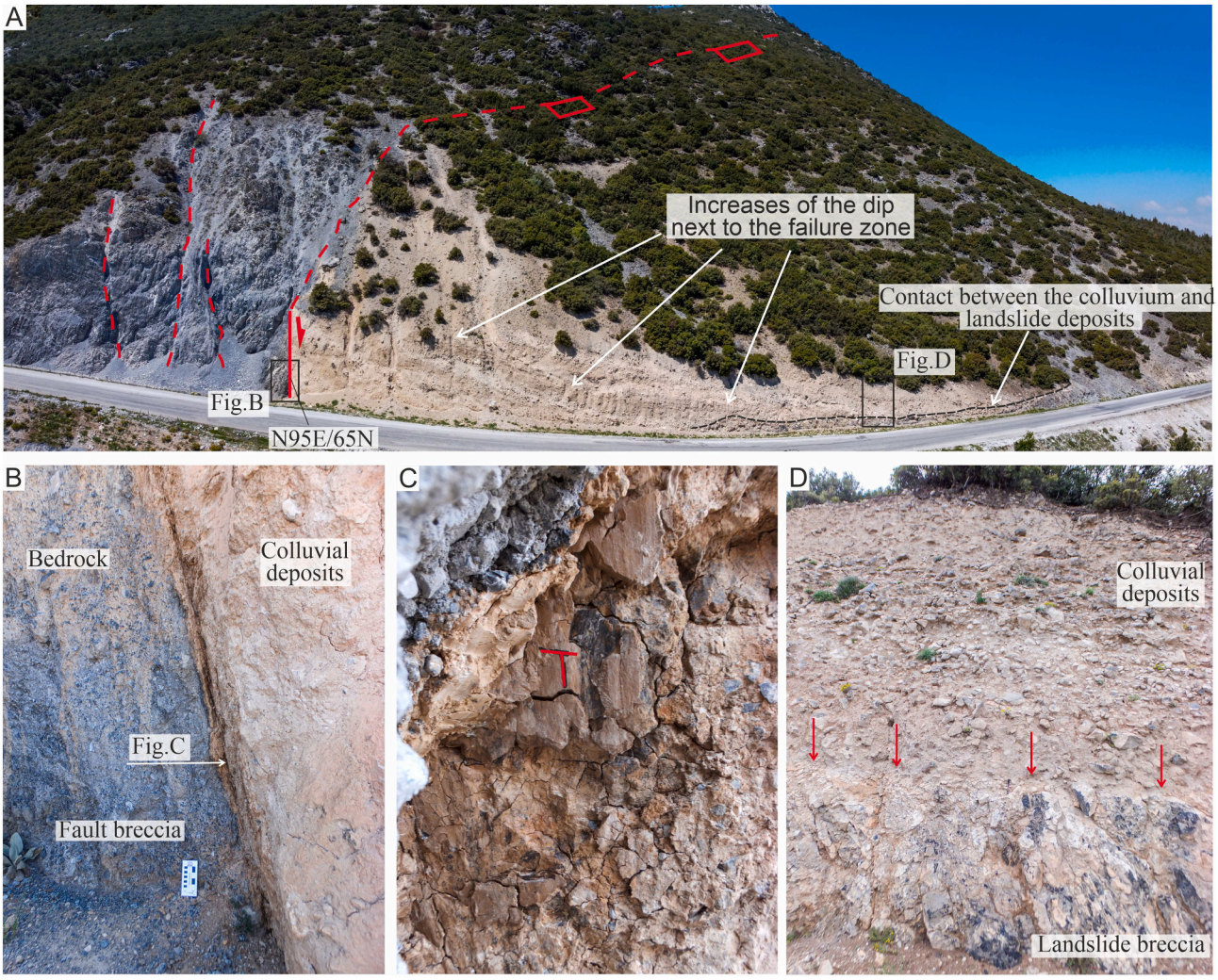

Fig. 15. A. Image showing the road-cut exposure at the eastern edge of landslide LsSW2. See Fig. 14 for location. The fault which controls a downhill-facing scarp is observed. The fault juxtaposes brecciated bedrock against colluvial deposits (talus), in turn underlain by a landslide breccia. The colluvial deposits exhibit evidence of fault dragging. B. Detailed view of the fault with a well-defined shear zone and a strongly comminuted fault breccia in the footwall. C. Close-up view of the fault surface with striated secondary carbonate. D. A Close-up view of the contact between the dilated landslide breccia and the overlying colluvial deposits marked by red arrows.

earthquakes with impact on slope stability. Seismicity associated with the Acıgöl Fault is evidenced by the M_w 5.8 earthquake that occurred on 08.08.2019. Paleoearthquakes have been identified via trenching on the Acıgöl and Maymundağı faults, although the ages of these events remain unpublished (Kürçer et al., 2016; Özdemir et al., 2017). The epicenter of the 1914, M_w 6.9 earthquake (Kılıç et al., 2017) was located around 25 km southeast of the investigated slopes, within the Burdur Graben. Similarly, the 1995, M_w 6.4 earthquake (Kılıç et al., 2017) was located about 30 km northeast from the studied slopes, within the Dinar Graben. The seismic activity in the area may also have played a role in triggering landslides on the Söğüt Mountain. Rodríguez et al. (1999), based on a large database of coseismic landslides, show that earthquakes within the magnitude range 6.5–7 can trigger landslides at a maximum distance of around 100 km, and that most of the slope movements occur at <20 km from the fault trace.

6.3. Relationship between tectonic and gravitational faults

As illustrated in the neotectonic grabens of the Apennines (Italy), normal faults in the basin margins can create relief and function as potential sliding planes with favorable orientation and low residual strength (Galadini, 2006; Gori et al., 2014). Thus, the upper portion of these faults can experience both tectonic and gravitational displacement. The development of gravitational failures taking advantage of tectonic faults seems to occur on landslides LsC2 and LsC3, with downhill-facing scarps several hundred meters high attributable to the superposition of tectonic and gravitational displacement (Fig. 10). This seems also to be the case for landslides LsSW1 and LsSW2 in the southwestern sector as supported by the following lines of evidence (Fig. 13): (1) the fault traces (Akgöl and Acıgöl faults) coincide with the head of the landslides; (2) anomalously large height of the head scars, related to the superposition of tectonic and gravitational deformation, with no mass balance between the depletion and accumulation zones of the landslides; (3) the exposure associated with the head of landslide LsSW2 reveals that the upper edge of this landslide coincides with an active normal fault that has offset both the landslide deposits and overlying talus deposits, likely of Holocene age (Fig. 15). The OSL age of the basin sediments overlain by the deposits of landslide LsSW2 indicate that the landslide postdates 24.1 ± 4.4 ka. Landslides LsC2 and LsC3 in the central sector likely share a similar age, considering that they have buried the eastern counterparts of the dated basin sediments. Landslide LsC3 should relatively younger based on cross-cutting relationships; its head scar affects landslide LsC2 (Fig. 10). Interestingly, the landslides controlled by active normal faults on the southeast margin of the Acıgöl

Fig. 16. A. Images showing the road-cut exposures along the valley east of landslide LsSW2. See Figs. 13 and 14 for location. B. Image of the eastern road cut showing angular colluvial deposits (talus) in fault contact with limestone. C. Image of the western exposure showing a monoclinal fold on alluvial fan deposits ascribable to a buried S-dipping secondary fault. Red circle indicates person for scale.

Graben reach gigantic dimensions (e.g., LsSW2, 3.5 Gm^3). Their large size is one of the reasons why these huge slope movements are often overlooked in geological maps (Cotton, 1999).

The slopes in the northeastern sector associated with the Acıgöl Fault do not display a distinct bulge penetrating into the basin, but a linear front-piedmont junction, two major downhill facing scarps and numerous sackung-like scarps and troughs extending from the ridge crest to the lower part of the mountain front (Figs. 7, 8A, 9A). The linear cartographic trace and high relief (300 m and 480 m) of the downhill-facing scarps strongly suggest that these are largely fault scarps created by normal faults, which may also have some gravitational displacement component. In fact, the upper downhill-facing scarp occurs along the projection of the basin-bounding fault segment east of its left-stepping stepover. The hectometer-scale throw on these ruptures cannot be explained solely by gravitational slope deformation. Normally, such significant displacement would involve the development of a well-defined landslide toe with significant runout. However, the absence of these features suggests that tectonic activity is contributing to the observed throw (resulting in a mass balance inconsistency). A number of studies document an upslope propagation of the surface ruptures (e.g., antislope scarps) in the slopes of glacial valleys affected by gravitational slope deformation (Pánek et al., 2017; McCalpin and Corominas, 2019). However, in the northeastern sector of the Söğüt Mountains geomorphic evidence indicates two domains bounded by the downhill-facing scarps with the opposite chronological sequence (i.e. younger slope deformation in the lower part). The more degraded appearance of the upper downhill-facing scarp clearly indicates its earlier formation. Additionally, the upper domain displays a more mature karst with a higher density of solution sinkholes, indicating an earlier onset of gravitational deformation, internal drainage and sinkhole formation in this zone. This temporal and spatial distribution is consistent with the slow formation process of solution sinkholes in carbonate rocks (e.g., De Waele and Gutiérrez, 2022), and their associated generation with gravitational deformation. This chronosequence is also evident in the morphometric properties of the gravitational deformations. In the lower part uphill-facing scarps are longer and the associated troughs are around six times larger and display a more youthful appearance. The apparently unusual downslope migration of the deformation observed in the northeastern sector of the study area could be related to the fact that the creation of the slope and its topographic growth is related to the activity of a normal fault located along its foot, which has two main implications: (1) debuttressing related to fault displacement mainly affects to the rock mass situated in the lower part of the slope, which progressively moves to a relatively higher position; and (2) the slope is a time-transgressive geomorphic surface, progressively younger towards the lower part (Fig. 17A, B). The scenario can be complicated if the tectonic deformation is caused by the activity of a master fault at the foot of the mountain front and secondary synthetic faults in the footwall, as seems to be the case in the Söğüt Mountains.

6.4. Evolution of DSGSDs

The work carried out suggests that the features mapped in the Söğüt Mountains represent different stages of an evolutionary trend, whereby DSGSDs mainly expressed by uphill-facing scarps and ridge-top

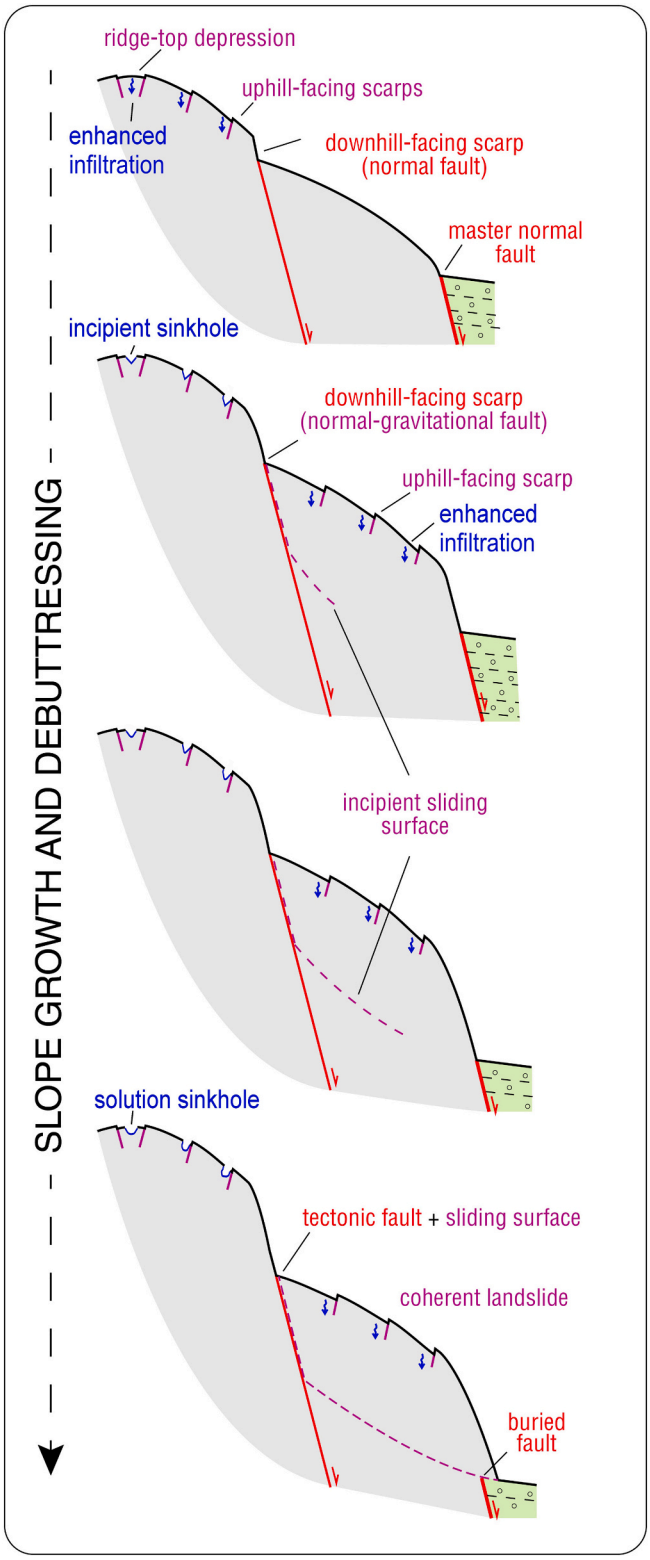

Fig. 17. Sketch illustrating the morphological evolution of the DSGSDs and short-runout landslides in the mountain front of grabens, where slopes experience long-term growth and debuttressing related to normal fault activity. The sliding surfaces can take advantage of favorably oriented synthetic normal faults with low residual strength.

depressions evolve into distinct large landslides with throughgoing sliding surfaces that may be guided by active synthetic normal faults (Fig. 17). Our mapping provides the opportunity to apply the ergodic concept, substituting space by time. The northeastern sector represents a DSGSD with numerous uphill facing scarps and two major downhill-facing scarps probably controlled by secondary tectonic faults (Fig. 7). The lack of a bulge at the foot of the slope, common in DSGSDs, could be related to the brittle rheology of the bedrock, plus continuous rejuvenation of the slope by faulting. The large landslides with uphill-facing scarps mapped in the central and southwestern sector of the range are very likely former DSGSDs that have evolved into distinct landslides with their failure plane guided in the upper part by normal faults (Fig. 17B, C). The DSGSD has contributed to reduce the overall rock mass strength (Pánek and Klimeš, 2016) until the formation of break out failure planes at the foot of the slopes. The landslide bodies have experienced limited basinward runout maintaining the coherence of the rock mass as indicates the presence of numerous uphill-facing scarps (Fig. 17D). The detachment of the landslide mass probably had a debuttressing effect on the higher sections of the slope, inducing the development or rejuvenation of scarps and depressions (e.g., McCalpin and Hart, 2002). The concept of DSGSD maturation and their evolution into large landslides has been proposed by a number of authors (e.g., McCalpin and Hart, 2002; Gutiérrez et al., 2008; Lebourg et al., 2011; Pánek and Klimeš, 2016; Agliardi and Crippa, 2022) and supported by statistical analyses in central Japan (Kaneda and Kono, 2017). Notably, recent instances of catastrophic slope failures occurring on slopes affected by DSGSDs have been documented (Wang et al., 2003; Chigira et al., 2003; Sakals et al., 2012; Nishii et al., 2013), further supporting that these are stages of a long-term slope evolution.

6.5. *Development of solution sinkholes*

The Söğüt Mountains show a high density of solution sinkholes despite the high overall gradient of the slopes. Here, sinkholes tend to show elongated geometries and alignments. The development of these features is favored by: (1) the formation of internally drained troughs by DSGSD with enhanced infiltration; and (2) strong fracturing and dilation of the carbonate bedrock by both tectonic and gravitational deformation. This combination of factors and processes result in the development of peculiar solution sinkholes superimposed on topographic lows created by gravitational deformation (i.e., polygenetic sinkholes).

7. Conclusions

This study provides geomorphic evidence of Quaternary activity on basin-bounding and intra-basin faults of the Acıgöl and Akgöl grabens in the West Anatolian extensional province. The southwestern sector of the Acıgöl Graben floor is compartmentalized into a series of half-graben depressions with conspicuous geomorphic expression that control the intra-basin hydrology. The unusually well-displayed topographic expression of the intra-basin faults is largely attributed to low aggradation rate related to limited runoff and sediment flux from the southeastern margin of the basin, underlain by karstified carbonate bedrock with slopes disrupted by DSGSD and large landslides.

The analysis of the DSGSDs and large landslides in the fault-bounded Söğüt Mountains, including detailed mapping, reveals a complex interplay between gravitational deformation and active faulting. The main predisposing and preparatory factors that contribute to the development of the slope failures include: (1) weakened rocks by fracturing and dilation related to ongoing tectonic and gravitational deformation; (2) laterally unconfined rock masses associated with bends and stepovers in the basin-bounding faults; and (3) steep and high relief slopes that experience long-term rejuvenation and debuttressing by displacement on normal faults along their foot. Ground shaking enhanced by topographic amplification related to large earthquakes sourced from onsite or the multiple offsite active normal faults, is likely the main triggering

factor for slope instability. Trenching and geochronological investigations aimed at dating and correlating displacement events in the DSGSDs and cosiesmic surface ruptures in the main faults would sight light on this issue, with practical implications for seismic hazard assessment in the region.

A multi-stage evolutionary sequence is inferred for the slope movements in the Söğüt Mountains, progressing from DSGSDs into distinct large, short-runout landslides: (1) slopes with ridge-top depressions and uphill-facing scarps in the upper part; (2) generation of younger uphill-facing scarps at lower elevation, where bedrock is newly exposed and debuttresed by fault activity; and (3) development of distinct landslides whose sliding surface is controlled in the upper part by active synthetic normal faults with both gravitational and tectonic displacement. This work documents for the first time sackung-type features and gigantic landslides (>1 Gm^3) in Türkiye. The findings of this study can be further developed through the acquisition of geochronological data and by applying numerical mechanical models as well as analog physical models.

The high density of elongated solution sinkholes forming alignments observed in the slopes of the Söğüt Mountains is largely related to favorable topographic and hydrological conditions created by DSGSDs (i.e., internally drained troughs).

CRediT authorship contribution statement

Esra Tunçel: Writing – review & editing, Writing – original draft, Visualization, Investigation, Funding acquisition, Conceptualization. **Francisco Gutiérrez:** Writing – review & editing, Visualization, Supervision, Investigation, Conceptualization. **Ergin Gökkaya:** Writing – review & editing, Investigation, Conceptualization. **Gürol Seyitoğlu:** Writing – review & editing, Supervision, Conceptualization. **İhsan Çiçek:** Writing – review & editing, Supervision, Funding acquisition, Conceptualization.

Declaration of competing interest

The authors declare that they have no known competing financial interests or personal relationships that could have appeared to influence the work reported in this paper.

Data availability

No data was used for the research described in the article.

Acknowledgements

This work is financially supported by Ankara University Scientific Research Project (21L0649002). The first author is thankful to Harun Tunçel for his assistance during the field campaigns, to Cengiz Yıldırım for his suggestions during the study, and to Eren Şahiner for analyzing OSL data. The work by FG has been supported by the project DIAPERNO (PID2021-123189NB-I00) of the Spanish Government (Ministerio de Ciencia e Innovación).

References

Agliardi, F., Crippa, C., 2022. Deep-Seated Gravitational Slope Deformations, Treatise on Geomorphology, 2nd edition. Elsevier, pp. 183–199.
Agliardi, F., Crosta, G., B and Frattini, P., 2012. Slow rock-slope deformation. Landslides: (Types, mechanisms and modeling: 207).
Agliardi, F., Crosta, G. and Zanchi, A., 2001. Structural constraints on deep-seated slope deformation kinematics. Eng. Geol., 59(1–2): 83–102.
Agliardi, F., Crosta, G.B., Zanchi, A., Ravazzi, C., 2009. Onset and timing of deep-seated gravitational slope deformations in the eastern Alps. Italy. Geomorphology 103 (1), 113–129.
Alçiçek, H., 2009. Late Miocene nonmarine sedimentation and formation of magnesites in the Acıgöl Basin, southwestern Anatolia. Turkey. Sedimentary Geology 219 (1–4), 115–135.
Alçiçek, M.C., Brogi, A., Capezzuoli, E., Liotta, D. and Meccheri, M., 2013. Superimposed basin formation during Neogene–Quaternary extensional tectonics in SW-Anatolia (Turkey): insights from the kinematics of the Dinar Fault Zone. Tectonophysics, 608: 713–727.
Altunel, E., Barka, A.A., Akyüz, H.S., 1999. Paleoseismology of Dinar Fault, SW Turkey. Terra Nova 11, 297–302.
Ambrosi, C. and Crosta, G.B., 2006. Large sackung along major tectonic features in the Central Italian Alps. Engineering geology, 83(1–3): 183–200.
Anda, E., Blikra, L.H., Braathen, A., 2002. The Berill Fault-first evidence of neotectonic faulting in southern Norway. Norwegian Journal of Geology/Norsk Geologisk Forening 82 (3).
Anders, M.H., Schlische, R.W., 1994. Overlapping faults, intrabasin highs, and the growth of normal faults. J. Geol. 102 (2), 165–179.
Arai, N., Chigira, M., 2019. Distribution of gravitational slope deformation and deep-seated landslides controlled by thrust faults in the Shimanto accretionary complex. Engineering geology 260, 105236.
Başarır, B.N., Özel, N.M., Altınok, Y. and Duman, T.Y., 2017. Türkiye ve yakın çevresi için geliştirilmiş tarihsel dönem (MÖ 2000 - MS 1900-) deprem katalogu. Türkiye Sismotektonik Haritası Açıklama Kitabı (Ed. T.Y. Duman), Maden Tetkik ve Arama Genel Müdürlüğü, Özel Yayınlar Serisi- 34, Ankara-Türkiye.
Bayer Altın, T., Kayseri-Özer, M.S., Altın, B.N., 2021. The Holocene terraces of the desiccated Bor Lake and Neolithic occupation in Bor Plain, Central Anatolia. Turkey. Environmental Earth Sciences 80 (16), 525.
Beck, A.C., 1968. Gravity faulting as a mechanism of topographic adjustment. N. Z. J. Geol. Geophys. 11 (1), 191–199.
Bovis, M.J., 1982. Uphill-facing (antislope) scarps in the Coast Mountains, Southwest British Columbia. Geol. Soc. Am. Bull. 93 (8), 804–812.
Břežný, M., Pánek, T., Lenart, J., Grygar, R., Táborík, P., McColl, S.T., 2018. Sackung and enigmatic mass movement folds on a structurally-controlled mountain ridge. Geomorphology 322, 175–187.
Burbank, D.W., Anderson, R.S., 2008. Tectonic Geomorphology. Blackwell Publishing.
Carbonel, D., Gutiérrez, F., Linares, R., Roqué, C., Zarroca, M., McCalpin, J., Rodríguez, V., 2013. Differentiating between gravitational and tectonic faults by means of geomorphological mapping, trenching and geophysical surveys. The case of the Zenzano Fault (Iberian Chain, N Spain). Geomorphology 189, 93–108.
Cartwright, J.A., Trudgill, B.D., Mansfield, C.S., 1995. Fault growth by segment linkage: an explanation for scatter in maximum displacement and trace length data from the Canyonlands Grabens of SE Utah. J. Struct. Geol. 17 (9), 1319–1326.
Chigira, M., 1992. Long-term gravitational deformation of rocks by mass rock creep. Engineering Geology 32 (3), 157–184.
Chigira, M., Wang, W.-N., Furuya, T., Kamai, T., 2003. Geological causes and geomorphological precursors of the Tsaoling landslide triggered by the 1999 Chi-Chi earthquake. Taiwan. Engineering Geology 68 (3–4), 259–273.
Chigira, M., Wu, X., Inokuchi, T., Wang, G., 2010. Landslides induced by the 2008 Wenchuan earthquake, Sichuan. China. Geomorphology 118 (3–4), 225–238.
Collins, A.S., Robertson, A.H., 1998. Processes of late cretaceous to late Miocene episodic thrust-sheet translation in the Lycian Taurides, SW Turkey. J. Geol. Soc. London 155 (5), 759–772.
Cotton, W., 1999. Faults aren't Always What they're Cracked up to Be. Techniques for Identifying Faults and Determining their Origins: US Nuclear Regulatory Commission, Washington, contract report NUREG/CR-5503, pp. A-29–A-50.
Cotton, W., Fowler, W., Van Velsor, J., 1989. Coseismic bedding plane faults and ground fissures associated with the Loma Prieta earthquake of 17 October 1989. The Loma Prieta (Santa Cruz Mountains), California, earthquake of 17 October 1989: California Division of Mines and Geology. Special Publication 104, 95–103.
Cowie, P., 1998a. A healing–reloading feedback control on the growth rate of seismogenic faults. Journal of Structural Geology 20 (8), 1075–1087.
Cowie, P.A., 1998b. Normal fault growth in three dimensions in continental and oceanic crust. Geophysical Monograph-American Geophysical Union 106, 325–348.
Cowie, P.A., Scholz, C.H., 1992. Growth of faults by accumulation of seismic slip. J. Geophys. Res. Solid Earth 97 (B7), 11085–11095.
Cowie, P., Gupta, S., Dawers, N., 2000. Implications of fault array evolution for synrift depocentre development: insights from a numerical fault growth model. Basin Res. 12 (3–4), 241–261.
Crosta, G., Frattini, P., Agliardi, F., 2013. Deep seated gravitational slope deformations in the European Alps. Tectonophysics 605, 13–33.
Cruden, D.M., Varnes, D.J., 1996. Landslide Types and Processes. Landslides. National Academy Press, Washington, pp. 36–75.
Dawers, N.H., Underhill, J.R., 2000. The role of fault interaction and linkage in controlling synrift stratigraphic sequences: late Jurassic, Statfjord East area, northern North Sea. AAPG Bull. 84 (1), 45–64.
de Graciansky, P.C., 1972. Recherches géologiques dans le Taurus Lycien. Universite de Paris-Sud, Centre d'Orsay.
De Waele, J., Gutiérrez, F., 2022. Karst Hydrogeology, Geomorphology and Caves. John Wiley & Sons.
Delchiaro, M., Della Seta, M., Martino, S., Dehbozorgi, M., Nozaem, R., 2019. Reconstruction of river valley evolution before and after the emplacement of the giant Seymareh rock avalanche (Zagros Mts., Iran). Earth Surface. Dynamics 7 (4), 929–947.
Demircioğlu, D., Ecevitoğlu, B., Seyitoğlu, G., 2010. Evidence of a rolling hinge mechanism in the seismic records of the hydrocarbon-bearing Alaşehir graben, western Turkey. Pet. Geosci. 16 (2), 155–160.
Dewey, J., Şengöl, A.M.C., 1979. Aegean and surrounding regions: complex multiplate and continuum tectonics in a convergent zone. Geol. Soc. Am. Bull. 90 (1), 84–92.
Di Luzio, E., Saroli, M., Esposito, C., Bianchi-Fasani, G., Cavinato, G., Scarascia-Mugnozza, G., 2004. Influence of structural framework on mountain slope

deformation in the Maiella anticline (Central Apennines, Italy). Geomorphology 60 (3–4), 417–432.
Discenza, M., Esposito, C., Martino, S., Petitta, M., Prestininzi, A., Scarascia Mugnozza, G., 2011. The gravitational slope deformation of Mt. Rocchetta ridge (central Apennines, Italy): geological-evolutionary model and numerical analysis. Bull. Eng. Geol. Environ. 70, 559–575.
Dramis, F., Sorriso-Valvo, M., 1994. Deep-seated gravitational slope deformations, related landslides and tectonics. Engineering Geology 38 (3–4), 231–243.
Durcan, J.A., King, G.E., Duller, G.A., 2015. DRAC: Dose Rate and Age Calculator for trapped charge dating. Quat. Geochronol. 28, 54–61.
El Bedoui, S., Guglielmi, Y., Lebourg, T., Pérez, J.-L., 2009. Deep-seated failure propagation in a fractured rock slope over 10,000 years: the La Clapière slope, the south-eastern French Alps. Geomorphology 105 (3–4), 232–238.
Elmas, G., Seyitoğlu, G., Kazancı, N., Veysel, I., 2019. Syn-sedimentary tectonic markings in the Oligocene Datça-Kale-Acı Göl basin, western Anatolia. Bulletin of the Mineral Research and Exploration 160 (160), 1–20.
Erinç, S., Bener, M., Sungur, K., Göçmen, K., 1971. 12 Mayıs 1971 Burdur Depremi. İ.Ü, Coğrafya Enstitüsü Yayınları, İstanbul.
Esposito, C., Martino, S., Mugnozza, G.S., 2007. Mountain slope deformations along thrust fronts in jointed limestone: an equivalent continuum modelling approach. Geomorphology 90 (1–2), 55–72.
Eyidoğan, H., Barka, A., 1996. The 1 October 1995 Dinar earthquake. SW Turkey. Terra Nova 8 (5), 479–485.
Fioraso, G., 2017. Impact of massive deep-seated rock slope failures on mountain valley morphology in the northern Cottian Alps (NW Italy). J. Maps 13 (2), 575–587.
Forcella, F., Orombelli, G., 1984. Holocene slope deformations in Valfurva, Central Alps. Italy. Geografia Fisica e Dinamica Quaternaria 7 (2), 41–48.
Galadini, F., 2006. Quaternary tectonics and large-scale gravitational deformations with evidence of rock-slide displacements in the Central Apennines (Central Italy). Geomorphology 82 (3–4), 201–228.
Gawthorpe, R., Leeder, M., 2000. Tectono-sedimentary evolution of active extensional basins. Basin Research 12 (3–4), 195–218.
Gawthorpe, R.L., Jackson, C.A.-L., Young, M.J., Sharp, I.R., Moustafa, A.R., Leppard, C. W., 2003. Normal fault growth, displacement localisation and the evolution of normal fault populations: the Hammam Faraun fault block, Suez rift. Egypt. Journal of Structural Geology 25 (6), 883–895.
Glade, T., Crozier, M.J., 2005. The nature of landslide hazard impact. Landslide hazard and risk 41–74.
Göktaş, F., Çakmakoğlu, A., Tarı, E., Sütçü, Y., Sarıkaya, H., 1989. Çivril-Çardak arasının jeolojisi. Maden Tetkik ve Arama Genel Müdürlüğü 8701, 109.
Goldscheider, N., Chen, Z., Auler, A.S., et al., 2020. Global distribution of carbonate rocks and karst water resources. Hydrgeol. J. 28 (5), 1661–1677.
Gori, S., Falcucci, E., Dramis, F., Galadini, F., Galli, P., Giaccio, B., Messina, P., Pizzi, A., Sposato, A., Cosentino, D., 2014. Deep-seated gravitational slope deformation, large-scale rock failure, and active normal faulting along Mt. Morrone (Sulmona basin, Central Italy): Geomorphological and paleoseismological analyses. Geomorphology 208, 88–101.
Guglielmi, Y., Cappa, F., 2010. Regional-scale relief evolution and large landslides: Insights from geomechanical analyses in the Tinée Valley (southern French Alps). Geomorphology 117 (1–2), 121–129.
Gupta, A., Scholz, C.H., 2000. A model of normal fault interaction based on observations and theory. Journal of structural Geology 22 (7), 865–879.
Gürbüz, A., Boyraz, S., Ismael, M.T., 2012. Plio-Quaternary development of the Baklan–Dinar graben: implications for cross-graben formation in SW Turkey. Int. Geol. Rev. 54 (1), 33–50.
Gürer, Ö.F., Yılmaz, Y., 2002. Geology of the Ören and surrounding areas, SW Anatolia. Turk. J. Earth Sci. 11 (1), 1–13.
Gutiérrez, F., Ortuño, M., Lucha, P., Guerrero, J., Acosta, E., Coratza, P., Piacentini, D., Soldati, M., 2008. Late Quaternary episodic displacement on a sackung scarp in the central Spanish Pyrenees. Secondary paleoseismic evidence? Geodin. Acta 21 (4), 187–202.
Gutiérrez, F., Carbonel, D., Guerrero, J., McCalpin, J., Linares, R., Roque, C., Zarroca, M., 2012a. Late Holocene episodic displacement on fault scarps related to interstratal dissolution of evaporites (Teruel Neogene Graben, NE Spain). Journal of Structural Geology 34, 2–19.
Gutiérrez, F., Linares, R., Roqué, C., Zarroca, M., Rosell, J., Galve, J., Carbonel, D., 2012b. Investigating gravitational grabens related to lateral spreading and evaporite dissolution subsidence by means of detailed mapping, trenching, and electrical resistivity tomography (Spanish Pyrenees). Lithosphere 4 (4), 331–353.
Gutiérrez, F., Sevil, J., Migoń, P., 2023. Landslides in the Remolinos gypsum escarpment (NE Spain): controls imposed by stratigraphy, fluvial erosion, and interstratal salt dissolution. Landslides 20 (10), 2075–2093.
Gutiérrez-Santolalla, F., Acosta, E., Ríos, S., Guerrero, J., Lucha, P., 2005. Geomorphology and geochronology of sackung features (uphill-facing scarps) in the Central Spanish Pyrenees. Geomorphology 69 (1–4), 298–314.
Hart, E.L., Bryant, W.A., Wills, C.J., Treiman, J.A., 1989. The search for fault rupture and significance of Ridgetop fissures, Santa Cruz Mountains, California. The Loma Prieta (Santa Cruz Mountains), California, earthquake of 17 October 1989: California Division of Mines and Geology. Special Publication 104, 83–94.
Helvacı, C., Alçiçek, M.C., Gündoğan, İ., Gemici, Ü., 2013. Tectonosedimentary development and palaeoenvironmental changes in the Acıgöl shallow-perennial playa-lake basin, SW Anatolia. Turkey. Turkish Journal of Earth Sciences 22 (2), 173–190.
Hovius, N., Meunier, P., Clague, J., Stead, D., 2012. Earthquake ground motion and patterns of seismically induced landsliding. Landslides: types, mechanisms and modeling. Cambridge University Press, Cambridge 3, 24–36.
Jaboyedoff, M., Penna, I., Pedrazzini, A., Baroň, I., Crosta, G.B., 2013. An introductory review on gravitational-deformation induced structures, fabrics and modeling. Tectonophysics 605, 1–12.
Jackson, J., 1999. Fault death: a perspective from actively deforming regions. Journal of Structural Geology 21 (8–9), 1003–1010.
Jackson, J., White, N., 1989. Normal faulting in the upper continental crust: observations from regions of active extension. Journal of Structural Geology 11 (1–2), 15–36.
Jibson, R.W., Harp, E.L., Schulz, W., Keefer, D.K., 2004. Landslides triggered by the 2002 Denali Fault, Alaska, earthquake and the inferred nature of the strong shaking. Earthq. Spectra 20 (3), 669–691.
Kadirioğlu, F., Kartal, R., Kılıç, T., Kalafat, D., Duman, T., Eroğlu Azak, T., Özalp, S. and Emre, Ö., 2017. Türkiye ve yakın çevresi için geliştirilmiş aletsel dönem (1900-2012) deprem kataloğu (M≥ 4, 0). Türkiye Sismotektonik Haritası Açıklama Kitabı (Ed. TY Duman). Maden Tetkik ve Arama Genel Müdürlüğü Özel Yayınlar Serisi-34, 1246.
Kaneda, H., Kono, T., 2017. Discovery, controls, and hazards of widespread deep-seated gravitational slope deformation in the Etsumi Mountains, Central Japan. J. Geophys. Res. Earth 122 (12), 2370–2391.
Kazancı, N., Boyraz, S., Özkul, M., Alçiçek, M.C., Kadıoğlu, Y., 2012. Late Holocene terrestrial tephra record at western Anatolia, Turkey: possible evidence of an explosive eruption outside Santorini in the eastern Mediterranean. Global Planet. Change 80, 36–50.
Kellerer-Pirklbauer, A., Gärtner-Roer, I., Bodin, X., Paro, L., 2022. European Alps. In: Oliva, M., Nývlt, D., Fernández-Fernández, J.M. (Eds.), Periglacial Landscapes of Europe. Springer International Publishing, Cham, pp. 147–224.
Kılıç, T., Kartal, R.F., Kadirioğlu, F.T., Duman, T.Y., Özalp, S., 2017. Türkiye ve yakın çevresi için düzenlenmiş moment tensor (1906–2012) kataloğu MW ≥ 4,0). In: Duman, T.Y. (Ed.), Türkiye Sismotektonik Haritası. Maden Tetkik ve Arama Genel Müdürlüğü, Özel Yayınlar Serisi-34, Ankara- Türkiye.
Koçyiğit, A., Gürboğa, D.Ş., 2010. Akgöl (Burdur) grabeninin neotektonik özellikleri ve kenar faylarının depremselliği. Türkiye Bilimsel ve Teknik Araştırma Kurumu, Ankara, Türkiye.
Komura, K., Kaneda, H., Tanaka, T., Kojima, S., Inoue, T., Nishio, T., 2020. Synchronized gravitational slope deformation and active faulting: a case study on and around the Neodani fault, Central Japan. Geomorphology 365, 107214.
Koral, H., 2000. Surface rupture and rupture mechanism of the October 1, 1995 (Mw= 6.2) Dinar earthquake, SW Turkey. Tectonophysics 327 (1–2), 15–24.
Krieger, I., Hermanns, R.L., Schleier, M., Molina, F.X.Y., Oppikofer, T., Ronning, J.S., Eike, T., Rohn, J., 2013. The Berill fault and its relation to a deep seated gravitational slope deformation (DSGSD). Italian journal of engineering geology and environment 265–273.
Kürçer, A., Olgun, Ş., Özdemir, E., Çan, T., Elmacı, H., 2016. Maymundağı Fayı'nda (Acıgöl Grabeni) Paleosismolojik Çalışmalar, GB Anadolu, Türkiye. In: Aktif Tektonik Araştırma Grubu 20. Kitabı/Proceedings book, Çalıştayı Bildiri Özleri.
Kürçer, A., Özdemir, E., Olgun, Ş., Özalp, S., Çan, T., Elmacı, H., 2021. Active tectonic and paleoseismological characteristics of the Dinar Fault, SW Anatolia. Turkey. Mediterranean Geoscience Reviews 3 (2), 219–251.
Kuzucuoğlu, C., Çiner, A., Kazancı, N., 2019. The geomorphological regions of Turkey. Landscapes and landforms of Turkey 41–178.
Le Pichon, X., Angelier, J., 1979. The Hellenic arc and trench system: a key to the neotectonic evolution of the eastern Mediterranean area. Tectonophysics 60 (1–2), 1–42.
Lebourg, T., Mickael, H., Hervé, J., Samyr, E.B.B., Thomas, B., Swann, Z., Emmanuel, T., Maurin, V., 2011. Temporal evolution of weathered cataclastic material in gravitational faults of the La Clapiere deep-seated landslide by mechanical approach. Landslides 8, 241–252.
Leeder, M., Gawthorpe, R., 1987. Sedimentary models for extensional tilt-block/half-graben basins. Geol. Soc. Lond. Spec. Publ. 28 (1), 139–152.
Leeder, M., Jackson, J., 1993. The interaction between normal faulting and drainage in active extensional basins, with examples from the western United States and Central Greece. Basin Res. 5 (2), 79–102.
Liang, P., Forman, S.L., 2019. LDAC: an Excel-based program for luminescence equivalent dose and burial age calculations. Ancient TL 37, 21–40.
Livio, F., Zerboni, A., Ferrario, M., Mariani, G., Martinelli, E., Amit, R., 2022. Triggering processes of deep-seated gravitational slope deformation (DSGSD) in an un-glaciated area of the Cavargna Valley (Central Southern Alps) during the Middle Holocene. Landslides 19 (8), 1825–1841.
Maffei, A., Martino, S., Prestininzi, A., 2005. From the geological to the numerical model in the analysis of gravity-induced slope deformations: an example from the Central Apennines (Italy). Engineering Geology 78 (3–4), 215–236.
McCalpin, J.P., 1999. Criteria for determining the seismic significance of sackungen and other scarplike landforms in mountainous regions. Techniques for Identifying Faults and determining their Origins. US Nuclear Regulatory Commission, Washington: 2.55-2.59.
McCalpin, J.P., Corominas, J., 2019. Postglacial deformation history of sackungen on the northern slope of Pic d'Encampadana, Andorra. Geomorphology 337, 134–150.
McCalpin, J.P., Hart, E.W., 2002. Ridge-top spreading features and relationship to earthquakes, San Gabriel Mountains Region, Southern California: Part a. distribution and description of ridge-top depressions (sackungen): Part B. Paleoseismic investigations of ridge-top depressions. Ridge-Top Spreading in California: California Geological Survey, Open-File Report 1.
McCalpin, J.P., Irvine, J.R., 1995. Sackungen at the Aspen Highlands ski area, Pitkin County. Colorado. Environmental & Engineering Geoscience 1 (3), 277–290.
McCalpin, J.P., Jones, L.C., 2021. The Stillwater Scarp, Central Nevada, USA; Coseismic Gravitational failure on a 1.200-M-High Range-Front Escarpment. Environ. Eng. Geosci. 27 (4), 377–393.

McCalpin, J., Gutierrez, F., Bruhn, R., Guerrero, J., Pavlis, T., Lucha, P., 2020. Tectonic geomorphology and late Quaternary deformation on the ragged Mountain fault, Yakutat microplate, south coastal Alaska. Geomorphology 351, 106875.
McGill, G.E., Stromquist, A.W., 1979. The grabens of Canyonlands National Park, Utah: geometry, mechanics, and kinematics. J. Geophys. Res. Solid Earth 84 (B9), 4547–4563.
McKenzie, D., 1978. Active tectonics of the Alpine—Himalayan belt: the Aegean Sea and surrounding regions. Geophys. J. Int. 55 (1), 217–254.
Meulenkamp, J., Wortel, M., Van Wamel, W., Spakman, W., Strating, E.H., 1988. On the Hellenic subduction zone and the geodynamic evolution of Crete since the late Middle Miocene. Tectonophysics 146 (1–4), 203–215.
Moro, M., Saroli, M., Salvi, S., Stramondo, S., Doumaz, F., 2007. The relationship between seismic deformation and deep-seated gravitational movements during the 1997 Umbria–Marche (Central Italy) earthquakes. Geomorphology 89 (3–4), 297–307.
Moro, M., Saroli, M., Gori, S., Falcucci, E., Galadini, F., Messina, P., 2012. The interaction between active normal faulting and large scale gravitational mass movements revealed by paleoseismological techniques: a case study from Central Italy. Geomorphology 151-152, 164–174.
Murray, A.S., Wintle, A.G., 2003. The single aliquot regenerative dose protocol: potential for improvements in reliability. Radiat. Meas. 37 (4–5), 377–381.
Nelson, M.S., Gray, H.J., Johnson, J.A., Rittenour, T.M., Feathers, J.K., Mahan, S.A., 2015. User guide for luminescence sampling in archaeological and geological contexts. Adv. Archaeol. Pract. 3 (2), 166–177.
Nishii, R., Matsuoka, N., Daimaru, H., Yasuda, M., 2013. Precursors and triggers of an alpine rockslide in Japan: the 2004 partial collapse during a snow-melting period. Landslides 10, 75–82.
Okay, A.I., Tüysüz, O., 1999. Tethyan sutures of northern Turkey. Geol. Soc. Lond. Spec. Publ. 156 (1), 475–515.
Özdemir, M., Bahadır, M., 2009. Çölleşme Sürecinde Acıgöl (1970-2008). Coğrafya Dergisi(18), 1–20.
Özdemir, E., Olgun, Ş., Çan, T., Tekin, S., Kürçer, A., Elmacı, H., 2017. Acıgöl Grabeni'nde İlk Paleosismolojik Çalışmalar, Güneybatı Türkiye. In: Aktif Tektonik Araştırma Grubu 21. Kitabı/Proceedings book, Çalıştayı Bildiri Özleri.
Özpolat, E., Şahiner, E., Özcan, O., Demir, T., Owen, L.A., 2021. Late-Holocene landscape evolution of a delta from foredune ridges: Seyhan Delta, Eastern Mediterranean. Turkey. The Holocene 31 (5), 760–777.
Özpolat, E., Yıldırım, C., Görüm, T., Gosse, J.C., Şahiner, E., Sarıkaya, M.A., Owen, L.A., 2022. Three-dimensional control of alluvial fans by rock uplift in an extensional regime: Aydın Range. Aegean extensional province. Scientific reports 12 (1), 15306.
Palmer, A.N., 1991. Origin and morphology of limestone caves. Geol. Soc. Am. Bull. 103 (1), 1–21.
Pánek, T., Klimeš, J., 2016. Temporal behavior of deep-seated gravitational slope deformations: a review. Earth Sci. Rev. 156, 14–38.
Pánek, T., Hradecký, J., Šilhán, K., Smolková, V., Altová, V., 2009. Time constraints for the evolution of a large slope collapse in karstified mountainous terrain of the southwestern Crimean Mountains. Ukraine. Geomorphology 108 (3), 171–181.
Pánek, T., Táborík, P., Klimeš, J., Komárková, V., Hradecký, J. and Šťastný, M., 2011. Deep-seated gravitational slope deformations in the highest parts of the Czech Flysch Carpathians: Evolutionary model based on kinematic analysis, electrical imaging and trenching. Geomorphology, 129(1–2): 92–112.
Pánek, T., Mentlík, P., Engel, Z., Braucher, R., Zondervan, A., Team, A., 2017. Late Quaternary sackungen in the highest mountains of the Carpathians. Quat. Sci. Rev. 159, 47–62.
Ponti, D.J., Wells, R.E., 1991. Off-fault ground ruptures in the Santa Cruz Mountains, California: Ridge-top spreading versus tectonic extension during the 1989 Loma Prieta earthquake. Bull. Seismol. Soc. Am. 81 (5), 1480–1510.
Prescott, J.R., Hutton, J.T., 1994. Cosmic ray contributions to dose rates for luminescence and ESR dating: large depths and long-term time variations. Radiat. Meas. 23 (2–3), 497–500.
Price, S.P., Scott, B., 1994. Fault-block rotations at the edge of a zone of continental extension; Southwest Turkey. J. Struct. Geol. 16 (3), 381–392.
Prosser, S., 1993. Rift-related linked depositional systems and their seismic expression. Geol. Soc. Lond. Spec. Publ. 71 (1), 35–66.
Radbruch-Hall, D., 1978. Gravitational creep of rock masses on slopes. In: B. Voight (Editor), Rockslides and Avalanches, 1.Natural Phenomena. Developments in Geotechnical Engineering. Elsevier, pp. 607–657.
Radbruch-Hall, D., Varnes, D., Savage, W., 1976. Gravitational spreading of steep-sided ridges (" sackung") in western United States. Bull. Int. Assoc. Eng. Geol. 13 (1), 23–35.
Rees, A., Thomas, A., Lewis, M., Hughes, H., Turner, P., 2014. Sequence stratigraphy, tectonostratigraphy and basin analysis. Geol. Soc. Lond. Mem. 42 (1), 101–134.
Reilinger, R., McClusky, S., Vernant, P., Lawrence, S., Ergintav, S., Cakmak, R., Ozener, H., Kadirov, F., Guliev, I., Stepanyan, R., 2006. GPS constraints on continental deformation in the Africa-Arabia-Eurasia continental collision zone and implications for the dynamics of plate interactions. J. Geophys. Res. Solid Earth 111 (B5).
Roberts, G.P., Michetti, A.M., 2004. Spatial and temporal variations in growth rates along active normal fault systems: an example from The Lazio–Abruzzo Apennines, central Italy. Journal of Structural Geology 26 (2), 339–376.
Robertson, A., Dixon, J., 1984. Introduction: aspects of the geological evolution of the Eastern Mediterranean. The Geological Society of London 1–74.
Rodríguez, C., Bommer, J., Chandler, R., 1999. Earthquake-induced landslides: 1980–1997. Soil Dyn. Earthq. Eng. 18 (5), 325–346.
Sakals, M.E., Geertsema, M., Schwab, J.W., Foord, V.N., 2012. The Todagin Creek landslide of October 3, 2006, Northwest British Columbia. Canada. Landslides 9 (1), 107–115.
Schleier, M., Hermanns, R.L.M., Krieger, I., Oppikofer, T., Eiken, T., Rønning, J.S., Rohn, J., 2016. Gravitational reactivation of a pre-existing post-Caledonian fault system: the deep-seated gravitational slope deformation at Middagstinden, western Norway. Nor. Geol. Tidsskr. 96 (3).
Şenel, M., 1997a. Geological maps of Turkey in 1: 100.000 scale, Denizli M23 sheet. Mineral Research and Exploration Directorate of Turkey (MTA), Ankara, Türkiye.
Şenel, M., 1997b. Geological maps of Turkey in 1: 100.000 scale, Isparta M24 sheet. Mineral Research and Exploration Directorate of Turkey (MTA), Ankara, Türkiye.
Şengör, A., 1987. Cross-faults and differential stretching of hanging walls in regions of low-angle normal faulting: examples from western Turkey. Geol. Soc. Lond. Spec. Publ. 28 (1), 575–589.
Şengör, A.C., Yılmaz, Y., 1981. Tethyan evolution of Turkey: a plate tectonic approach. Tectonophysics 75 (3–4), 181–241.
Şengör, A., Görür, N. and Şaroğlu, F., 1985. Strike-slip faulting and related basin formation in zones of tectonic escape: Turkey as a case study. In: Biddle, K. T., and Christie-Blick, N. (Editor) Strike-slip Deformation, Basin Formation, and Sedimentation, Soc. Econ. Paleontol. Miner. Spec. Publ. 37 (in honor of J.C. Crowell), pp. 227–64.
Seyitoğlu, G., Scott, B., 1991. Late Cenozoic crustal extension and basin formation in West Turkey. Geol. Mag. 128 (2), 155–166.
Seyítoğlu, G., Scott, B.C., 1996. The cause of NS extensional tectonics in western Turkey: tectonic escape vs back-arc spreading vs orogenic collapse. J. Geodyn. 22 (1–2), 145–153.
Seyitoğlu, G., Işık, V., Cemen, I., 2004. Complete Tertiary exhumation history of the Menderes massif, western Turkey: an alternative working hypothesis. Terra Nova 16 (6), 358–364.
Seyitoğlu, G., Aktuğ, B., Esat, K., Kaypak, B., 2022a. Neotectonics of Turkey (Türkiye) and surrounding regions: a new perspective with block modelling. Geologica acta: an international earth science journal 20 (1), 4.
Seyitoğlu, G., Tunçel, E., Kaypak, B., Korhan, E., Gökkaya, E., 2022b. The Anatolian Diagonal: a broad left-lateral shear zone between the North Anatolian Fault Zone and the Aegean/Cyprus arcs. Türk. Jeol. Bül. 65 (2), 93–116.
Sharp, I.R., Gawthorpe, R.L., Underhill, J.R., Gupta, S., 2000. Fault-propagation folding in extensional settings: examples of structural style and synrift sedimentary response from the Suez rift, Sinai. Egypt. Geological Society of America Bulletin 112 (12), 1877–1899.
Sickenberg, O., Tobien, H., 1971. New Neogene and lower Quaternary vertebrate faunas in Turkey. Newsl. Stratigr. 51–61.
Solonenko, V., 1977. Landslides and Collapses in Seismic Zones and their Prediction.
Sözbilir, H., Eski, S., Tepe, Ç., Duran, İ., Özkaymak, Ç., Tiryakioğlu, İ., Doğan, O., Akyar, B.E., 2019. 8 Ağustos 2019 Kuşadası Körfezi (İzmir) ve Bozkurt (Denizli) depremleri özet raporu.
Taymaz, T., Price, S., 1992. The 1971 May 12 Burdur earthquake sequence, SW Turkey: a synthesis of seismological and geological observations. Geophys. J. Int. 108 (2), 589–603.
Thomson, S.N., Stöckhert, B., Brix, M.R., 1998. Thermochronology of the highpressure metamorphic rocks of Crete, Greece: Implications for the speed of tectonic processes. Geology 26 (3), 259–262.
Trudgill, B.D., 2002. Structural controls on drainage development in the Canyonlands grabens of Southeast Utah. AAPG bulletin 86 (6), 1095–1112.
U.S. Geological Survey, 2023, Earthquake Lists, Maps, and Statistics, accessed September 20, 2023 at URL https://www.usgs.gov/natural-hazards/earthquake-hazards/lists-maps-and-statistics.
Ustaszewski, M., Pfiffner, O.A., 2008. Neotectonic Faulting, Uplift and Seismicity in the Central and Western Swiss Alps, 298. The Geological Society of London, London.
Varnes, D.J., Radbruch-Hall, D.H. and Savage, W.Z., 1989. Topographic and structural conditions in areas of gravitational spreading of ridges in the western United States. United States Geological Survey, Professional Paper;(USA), 1496.
Walsh, J.J., Watterson, J., 1988. Analysis of the relationship between displacements and dimensions of faults. J. Struct. Geol. 10 (3), 239–247.
Wang, W.N., Chigira, M., Furuya, T., 2003. Geological and geomorphological precursors of the Chiu-fen-erh-shan landslide triggered by the Chi-chi earthquake in Central Taiwan. Eng. Geol. 69 (1–2), 1–13.
Yilmaz, Y., Genç, Ş.C., Gürer, F., Bozcu, M., Yilmaz, K., Karacik, Z., Altunkaynak, Ş., Elmas, A., 2000. When did the western Anatolian grabens begin to develop? Geol. Soc. Lond. Spec. Publ. 173 (1), 353–384.
Zischinsky, U., 1969. Über sackungen. Rock Mechanics 1, 30–52.